1-1-1968

An experimental investigation of a two-dimensional turbulent jet flow over a rotating cylinder.

Helmut Keil
University of Windsor

AN EXPERIMENTAL INVESTIGATION OF A TWO - DIMENSIONAL TURBULENT JET FLOW OVER A ROTATING CYLINDER

A THESIS

Submitted to the Faculty of Graduate Studies through the Department of Mechanical Engineering in Partial Fulfilment of the requirements for the Degree of Master of Applied Science at the University of Windsor.

By

HELMUT KEIL

B. A. Sc., University of Windsor,

Windsor, Ontario, 1967.

Windsor, Ontario, Canada.

1968

Approved by: S. Lidman

Henry J. Huber

Ira Longanecker

SUMMARY

The flow of a two - dimensional turbulent jet over a rotating cylinder at different speeds was probed at various stations along the jet. The jet slot thickness and the velocity were kept constant. It was found that the velocity profiles were not similar at all downstream stations but only in the region where the maximum jet velocity was greater than the surface speed. When the surface speed became the maximum velocity, the jet could not be separated into an inner and outer layer. With the surface spinning in the direction of the jet, the angular position of jet separation initially increased with surface speed and reached a constant value. With opposite rotation it decreased linearly with surface speed.

ACKNOWLEDGEMENTS

The author is very grateful to Professor W. Colborne, Head of the Department of Mechanical Engineering, for having offered him the opportunity to pursue this investigation.

The author wishes to express his gratitude to Dr. K. Sridhar for his supervision, generous aid and encouragement throughout this work.

Thanks are also due to O. Brudy, P. Liebsch and R. Myers for their most helpful advice.

Work was made possible by the financial support of the National Research Council and the Defense Research Board of Canada.

TABLE OF CONTENTS

NOTATION

t	jet nozzle width (L)
Ro	radius of the cylinder (L)
a	constant in Table 2.1
b	constant in Table 2.1
u	tangential velocity component (L/T)
Us	surface speed (L/T)
Um	maximum value of u (L/T)
Um_2	maximum velocity Region II (L/T)
Uo	average jet velocity at nozzle exit (L/T)
U_1	square velocity profile (L/T)
y	coordinate normal to the surface (L)
y_m	value of y where u = Um (L)
$y_{m/2}$	larger value of y for which $u = \frac{1}{2}Um$ (L)
y_1	width of square velocity profile (L)
Y^1	non-dimensional distance ie. $\frac{y_{m/2}}{t}$
X^1	non-dimensional distance ie. $\frac{Ro\theta}{t}$
θ	angular position measured from the nozzle exit
θ_1	angular position measured from hypothetical origin
θo	$\theta_1 - \theta$
$\theta_{sep.}$	angular position of separation
α	yaw angle of the probe

Pa	atmospheric pressure (M/LT^2)
Ps	static pressure on the surface (M/LT^2)
P_T	total pressure in the flow (M/LT^2)
Pt	total pressure at the nozzle exit (M/LT^2)
Re	Reynolds number $= \left[\frac{(Pt - Pa)tRo}{e\,\nu^2}\right]^{\frac{1}{2}}$
ν	kinematic viscosity of the fluid (L^2/T)
e	density of the fluid (M/L^3)
Jo	actual jet momentum at the nozzle exit obtained by $\int_0^t e\,u^2\,dy$ (M/T^2)
N	speed of rotation in RPM (1/T)
w	speed of rotation $= 2\pi N$ (1/T)
K	coefficient of actual jet momentum emanating from the nozzle defined by Eq. 2.10

LIST OF FIGURES

CHAPTER 1

INTRODUCTION

The term "wall jet" as introduced by Glauert (Ref. 1) describes the flow of a jet along a straight wall when the pressure everywhere equals that of the surrounding fluid which is at rest. From common observations it is evident that jets, particularly plane, two - dimensional jets, show a strong tendency to attach and flow around a nearby solid surface. This phenomenon is usually called Coanda effect. The curved wall jet is then a jet flowing over a curved wall.

In all of the previous work on turbulent curved wall jets, the wall surface was stationary. Newman (Ref. 2), Nakaguchi (Ref. 3), and Fekete (Ref. 4) have done considerable work in this field. Only one reference (Ref. 5) has been found which considers an axi - symmetric jet impinging on a rotating disc. This is a theoretical study using a laminar jet.

Information obtained from the study would be useful for such applications as high lift and cooling devices.

In the case of cooling devices, the velocity profiles are essential for the study of the heat transfer characteristics.

The present investigation aims to provide information on the jet flow over a rotating cylinder. Since this is a preliminary study of the effects of rotation, the radius of the cylinder, jet slot width, and jet exit Reynolds number are kept constant.

CHAPTER II

LITERATURE SURVEY

The material covered in this chapter summarizes briefly the existing literature and is included in the report for the sake of completeness and ease of reference. The present investigation requires information on wall jets, primarily on jet flows over circular cylinders. A literature survey was done to obtain such information.

2.1 PLANE WALL JET

A jet flowing over a plane solid surface is called a plane wall jet (Fig. 2.1). In 1956 Glauert (Ref. 1) presented a theoretical analysis of the wall jet. By using Prandtl's hypothesis for the outer layer and Blasius' shear stress relation for the inner layer, he deduced that complete similarity was not possible. Glauert also determined that $U_m \propto x^a$ and $y_m/2 \propto x^b$. A number of investigators have experimentally found values of a and b as well as the power law of the inner layer as given in Table 2.1.

2.2 CURVED WALL JET

Newman did a dimensional analysis of the flow over a curved wall (Fig. 2.2) using the following variables: (Pa - Ps), (Pt - Pa), t, Ro, ρ, ν and θ. The pressure difference across the jet sheet (Pa - Ps) at an angular position θ may therefore be related non - dimensionally to these parameters as follows:

$$\left(\frac{Pa - Ps}{Pt - Pa}\right) = f\left\{\theta, \; {}^{t}/_{Ro}, \; \left[\frac{(Pt - Pa)\, Ro^2}{\rho \nu^2}\right]^{\frac{1}{2}}\right\} \qquad \ldots(2.1)$$

At some distance from the slot we might expect the flow to become dependent only on the product (Pt - Pa)t as long as a suitable zero is chosen for θ. Furthermore for large values of Reynolds number the flow will tend to become independent of viscosity so that:

$$\left(\frac{Pa - Ps}{Pt - Pa}\right) \cdot \frac{Ro}{t} = f(\theta) \qquad \ldots(2.2)$$

Similar results can be stated for the angular position of separation $\theta_{sep.}$ as follows:

$$\theta_{sep.} = f\left\{{}^{t}/_{Ro}, \left[\frac{(Pt - Pa)}{\rho \nu^2}\, tRo\right]^{\frac{1}{2}}\right\} \qquad \ldots(2.3)$$

If the position of separation is sufficiently far from the slot, then $\theta_{sep.}$ will depend only on Re.

$$\theta_{sep.} = f\left\{\left[\frac{(Pt - Pa)}{\rho \nu^2}\, tRo\right]^{\frac{1}{2}}\right\} \qquad \ldots(2.4)$$

At large Reynolds number with a suitably chosen zero, $\theta_{sep.}$ tends to become constant. For small values of

t/Ro, $\theta_{sep.}$ measured from the slot is 240 degrees for t/Ro values ranging from 0.02 to 0.4.

The maximum jet velocity coefficient is given by

$$\frac{\rho Um^2\, Ro\theta}{(Pt - Pa)t} = f\left\{ \theta,\ t/Ro,\ \left[\frac{(Pt - Pa)}{\rho \nu^2}\, tRo\right]^{\frac{1}{2}} \right\} \qquad \ldots(2.5)$$

For the growth law, Newman reasoned that analagous to the plane wall jet, the downstream distance x would be replaced by $(Ro + ky_{m/2})\theta$ where k is an unknown constamt of order unity. The growth law is then

$$\frac{y_{m/2}}{Ro\theta} = C\left[1 + \frac{k y_{m/2}}{Ro}\right] \qquad \ldots(2.6)$$

The values of C and k Newman found experimentally to be 0.11 and 1.5 respectively. Experimental results (Ref. 2) verify the above statements.

To get mathematical expressions for the surface pressure distribution, decay of the maximum velocity, and jet growth, Newman made the following assumptions:

1. The effect of skin friction on the jet momentum is small and negligible. Thus the sum of the moment of momentum and the moment of the pressure forces about the centre of the circular cylinder is constant.

2. The radial velocity is very much less than the circumferential velocity u so the centre of the streamlines are circles with centres at the centre of the cylinder (boundary layer approximation).

3. The velocity profiles U/Um vs. $y/y_{m/2}$ are the same

for all θ and may be replaced by a uniform velocity profile of the same mass flow and the same momentum.

4. Reynolds number is greater than 4×10^4.

The theoretical expression for the maximum velocity decay coefficient becomes:

$$\frac{\varrho U_m^2 \, R_o \theta}{(P_t - P_a) t} = \frac{128\theta}{9\left[\left\{\frac{4}{3}\frac{y_{m/2}}{R_o} + 1\right\}^2 - 1 + 2 \ln\left\{1 + \frac{4}{3}\frac{y_{m/2}}{R_o}\right\}\right]} \qquad \ldots(2.7)$$

where $y_{m/2}$ is related to θ by eq. 2.6. The surface pressure distribution is given as:

$$\left(\frac{P_a - P_s}{P_t - P_a}\right) \cdot \frac{R_o}{t} = \frac{8 \ln\left\{1 + \frac{4}{3}\frac{y_{m/2}}{R_o}\right\}}{\left\{\frac{4}{3}\frac{y_{m/2}}{R_o} + 1\right\}^2 - 1 + 2 \ln\left\{1 + \frac{4}{3}\frac{y_{m/2}}{R_o}\right\}} . \qquad \ldots(2.8)$$

Fekete made two refinements over Newman's theoretical expressions.

1. If the skin friction forces are neglible compared with the jet momentum, a suitable zero can be chosen for the angular position θ and a universal flow can be assumed to emanate from this hypothetical origin. From dimensional analysis, the hypothetical origin measured upstream is seen to depend on the following parameters:

$$\theta_o = f\left\{\frac{t}{R_o}, \left[\frac{(P_t - P_a)\, t R_o}{\varrho \nu^2}\right]^{\frac{1}{2}}\right\} \qquad \ldots(2.9)$$

2. The velocity profile of the jet at the exit is not uniform due to the boundary layer on the walls of the

nozzle. The coefficient of actual jet momentum emanating from the nozzle is then

$$K = \frac{Jo}{2(Pt - Pa)t} \qquad \ldots(2.10)$$

With these two refinements, equations 2.7 and 2.8 become:

$$\frac{\rho Um^2 \, Ro\theta_1}{K(Pt - Pa)t} = \frac{8\theta_1}{D^2\left[E\left\{ \frac{y_{m/2}}{Ro} + 1 \right\}^2 - 1 + 2\ln\left\{ E \frac{y_{m/2}}{Ro} + 1 \right\} \right]} \qquad \ldots(2.11)$$

$$\frac{(Pa - Ps)}{K(Pt - Pa)} \cdot \frac{Ro}{t} = \frac{8 \ln\left[E \frac{y_{m/2}}{Ro} + 1 \right]}{\left[E \frac{y_{m/2}}{Ro} + 1 \right]^2 - 1 + 2\ln\left[E \frac{y_{m/2}}{Ro} + 1 \right]} \qquad \ldots(2.12)$$

where $D = \frac{U_1}{Um}$ and $E = \frac{y_1}{y_{m/2}}$.

From dimensional reasoning the spread of the jet is

$$\frac{y_{m/2}}{Ro\theta_1} = f\left[\frac{y_{m/2}}{Ro}\right]$$

$$= d_o + d_1\left[\frac{y_{m/2}}{Ro}\right] + d_2\left[\frac{y_{m/2}}{Ro}\right]^2 + \ldots \qquad \ldots(2.13)$$

The hypothetical origin is found to be

$$\theta_o = C_1 \frac{t}{Ro} \qquad \ldots(2.14)$$

$$\text{and} \quad \theta_1 = \theta + \theta_o \qquad \ldots(2.15)$$

Taking the first two terms of eq. 2.13 and combining it with eq. 2.14 and 2.15, Fekete's growth law is

$$\frac{y_{m/2}}{Ro\left[\theta + \frac{t}{Ro}C_1\right]} = C\left[1 + k\frac{y_{m/2}}{Ro}\right] \qquad \ldots(2.16)$$

Experimental values of C_1, C, and k, Fekete found to be 2.93, 0.1004, and 1.839 using a Pitot tube at Re = 0.80×10^4.

Fekete found θ_{sep} to depend on surface roughness and was constant for Re > 4×10^4.

Nakaguchi made a theoretical analysis for incompressible flows by solving the Navier - Stokes equations of motion after making suitable assumptions (Ref. 3) to simplify them. Nakaguchi found that the velocity profiles which he assumed (half a free jet) agreed fairly well with the experimental results except in the minor part close to the wall surface. He theoretically developed the relationship for jet growth,

$$\frac{y_{m/2}}{Ro} = 0.040\theta^2 + 0.086\theta \qquad \ldots(2.17)$$

which agreed well with his experimental results. This jet growth law deviates rapidly from that given by Newman for θ values larger than about 160°. The formula for the local maximum jet velocity, Nakaguchi derived as

$$\frac{Um}{(Um)_1} = \left[\frac{y_{m/2}}{(y_{m/2})_1}\right]^n \qquad \ldots(2.18)$$

where $(Um)_1$ was the maximum jet velocity at some arbitrarily chosen point in the fully developed flow. This prediction is fairly satisfactory except in the vicinity of the jet slot

where the potential core remains. The value of n is approximately -0.5.

2.3 WALL JET ON MOVING SURFACE

A mathematical treatment of an axi - symmetric jet impinging on a rotating disc was given by Rarity in 1964. The flow is laminar and the jet impinges perpendicular to the flow surface and then spreads out radially.

In his analysis, the flow was treated as:

1. disc controlled - The flow was treated as a rotating disc problem with the jet adding disturbances to the flow.

2. jet controlled - The jet was strong compared to the speed of rotation of the disc and thus the jet was the main part of the flow.

This idea of having jet controlled or disc controlled flow was used in the selection of the repeating variables in a dimensional analysis of the present problem as seen in the appendix.

CHAPTER 111

TEST FACILITIES

A schematic diagram of the test facilities is shown in Fig. 3.1. Reference to the letter code used in Fig. 1 is made in the description of the test facilities.

3.1 AIR SUPPLY AND GUIDING DUCT

Air was supplied by a type HS, size 200 American standard centrifugal fan (A) with static pressure of 5 inches of water. This fan was driven by a 5 hp, 1745 RPM General Electric induction motor. A 30 inch long wooden guiding duct (B) with a rectangular cross - section was attached to the fan exit. A honey - comb flow straightener was placed in the guiding duct to reduce the turbulence level induced by the flow.

3.2 CONTRACTION DUCT AND NOZZLE

A wooden contraction duct (C) 30 inches long was placed after the guiding duct. An elbow (D) made of brass with uniform cross section of 2" x 9" turned the flow 90 degrees. The converging nozzle (E) also made of brass with

a 0.25" x 9" exit was attached to the flow. The contraction ratio for the nozzle and the duct were 62:1 in the 0.25" direction and 2.5:1 in the perpendicular direction. A Kiel probe with a 0.125" diameter shroud was placed in the contraction duct to measure air supply pressure.

3.3 ROTATING CYLINDER APPARATUS

The rotating cylinder and drive arrangement are shown in Fig. 3.2. The cylinder (F) consisted of a circular $\frac{1}{4}$" thick, 13.75" diameter acryllic plastic drum mounted to the rotating shaft by means of 3 Dodge 3/4" self alligning bearings. The end plates (H), with the two radii 2' and 3' to obtain two - dimensionality throughout, were fixed perpendicular to the shaft and consisted of 3/8" acryllic plastic supported around the edge by ten plastic poles 1" in diameter and 9" in length. The top end plate was prevented from sagging in the middle by a 3" x 4" x $\frac{1}{4}$" aluminum angle (I) which was fastened to the plate by means of screws. This also gave a firm mount for the top bearing and traversing arm.

The cylinder was driven by a $\frac{1}{2}$ hp General Electric 1 phase motor. The variable speed was obtained by moving the driving wheel (K) horizontally so that it was in contact with the wheel being driven (L) at various radii. This gave variable speed ranging from 125 to 1000 RPM with only two sizes of the driving wheel. The driving surface was nylon and the driven surface was rubber giving a minimum of noise and no noticeable wear. The speed of rotation was

found to be steady due to the inertia of the heavy aluminum discs. The speed was measured with a stroboscope having a range of 110 - 40,000 RPM, with an accuracy of 10 RPM.

The arm (M) on to which the probes were mounted was constructed so that measurements could be made at the 2' and 3' radius of the end plates. The arm was moved manually and could be placed accurately to the required angle since the circular end plate was evenly divided into 5 degree intervals. The traversing gear (J) which was mounted on to the arm could be moved parallel as well as perpendicular to the surface. In the perpendicular direction which was the most critical one, the traverse could be moved in 0.001" intervals by means of the commercial Helos dial calipers which were mounted into the traversing gear.

3.4 PROBING EQUIPMENT

A flattened stainless hypodermic tube with an opening of 0.002" by 0.066" was used to measure the total pressure in the jet.

The static pressure was obtained by means of two probes.

1. A flat static pressure probe as shown in Fig. 3.3b was used to measure the static pressure near the surface.

2. A disc probe as shown in Fig. 3.3c was used to measure the static pressure further away from the wall. The disc consisted of a $\frac{1}{2}$" brass disc with an opening of 0.021". The arm was brought out straight to insure a minimum of flow disturbance.

The pressure measurements were made with two variable sloping, single tube manometers with an accuracy of 0.001" of alcohol.

The position of flow separation was determined with a wool tuft probe (Fig. 3.3d). The tufts were between $1\frac{1}{2}$" to 2" in length and frayed at the end to assure maximum sensitivity to flow direction.

CHAPTER IV

EXPERIMENTS

The principal objectives of the experiments were to determine the effect of rotation of the wall on the flow of a jet over it. With Re and t/Ro equal to 6.6×10^4 and 0.036 respectively, studies were made of the velocity profiles, jet growth, maximum velocity decay, rotation opposite to the jet flow, and separation. The velocity profiles at the mid - span positions for various speeds of rotation were obtained first. The nozzle width, the jet velocity at the nozzle exit and the radius of the cylinder were all kept constant during the experiments. Speed of rotation was the important variable.

4.1 CALIBRATION

The flattened hypodermic tube used for measuring the total pressure was compared with a standard Pitot probe in uniform flow as well as in the jet flow and indicated good agreement. Fig. 4.1 shows the effect of yaw on the probe.

The disc static pressure probe was compared with a standard static pressure probe in a closed circuit wind tunnel. The results as shown in Fig. 4.2 indicate that

the disc gave true readings directly. The two static probes were checked for yaw characteristics and from Figs. 4.3 and 4.4 it was evident that the disc probe showed no yaw effect even at 45 degrees whereas the flat static probe was good only in the the range of ±5 degrees.

The velocity distribution across the nozzle width at different positions along the span was obtained. No significant changes in these profiles were noted with the spanwise centreline velocity distributions uniform over 95% of the nozzle. The velocity distribution at the mid-span, which was found to be uniform over 80% of the 0.25" width varying only ±1% from the central core velocity of 138 ft/sec., is seen in Fig. 4.5. The boundary layer on the cylinder side of the jet was much thinner than on the opposite side due to the centrifugal effect of the flow being turned by the elbow.

A check for two - dimensionality was done by investigating the velocity profiles at stations 2.0" above and below the centreline. All these velocity profiles overlapped (Fig. 4.6).

4.2 TEST PROCEDURE

4.2.1 VELOCITY PROFILES

After the nozzle and cylinder were aligned, the gap between them was sealed off by means of some gray adhesive. The cylinder thus rubbed gently against the tape and no significant amount of air could be sucked in by the jet.

The jet was then probed at six different stations along the wall ($30^{\circ} \leq \theta \leq 165^{\circ}$) and at six different

speeds of rotation ranging from 0 to 1000. Close to the surface the probe was traversed across the jet in intervals of 0.005" while further out, the intervals varied from 0.010" to 0.050" depending on the total pressure gradient present. The total pressure probe and disc probe were both mounted onto the traversing gear. With two sloping manometers, the static and total pressures for a given position could be taken at one setting of the traverse.

4.2.2 VISULIZATION OF FLOW SEPARATION

Using the tuft probe (Fig. 3.3d), flow separation data were obtained. The traversing arm was moved such that the wool tufts all fluctuated in the direction of the jet. The arm was then moved in the direction of increasing θ until it was noted that some tufts near the surface began to fluctuate back and forth. This position was recorded and the procedure repeated several times. By this method the separation angle was obtained within $\pm$ 3 degrees. When the cylinder was rotated in the opposite direction to the jet flow, the position of separation was more clearly evident and the angle obtained to within $\pm$ 2 degrees.

4.2.3 OPPOSITE ROTATION

The cylinder was rotated in the opposite direction to the jet flow by interchanging the leads in the motor. The jet was then probed at 4 different stations along the mid - span for a speed of 500 RPM and velocity profiles were obtained.

The angles of separation were obtained for 5

different speeds ranging from 125 to 700 RPM.

CHAPTER V

EXPERIMENTAL RESULTS

5.1 DATA REDUCTION

The fluid was treated as incompressible because the maximum velocity of the jet was only 138 ft/sec. From barometric pressure and room temperature the density of the air was determined. The experimental data were reduced with the help of an IBM 1620 computer and the output was plotted directly by an Alcomp plotter. Input data were room temperature, barometric pressure, manometer reading, y, Um, $y_{m/2}$. The plots of y vs. U, $\frac{y}{y_{m/2}}$ vs. $\frac{U}{Um}$, $\frac{(Pa - P)}{(Pt - Pa)} \cdot \frac{Ro}{t}$ vs. y were obtained as output information.

5.2 PRESENTATION AND DISCUSSION OF RESULTS

5.2.1 STATIC PRESSURE DISTRIBUTION

The static pressure distribution across the jet was found to be linear as seen in Fig. 5.1. The value obtained by extrapolation of the disc probe readings was about 1.16 times the value given by the flat static pressure probe placed at the surface. This factor agreed with previous

work (Ref. 11) done to compare the surface static pressure readings obtained with the flat static pressure probe and wall tap. The other deviations of the flat static probe from the linear pressure distribution is thought to be due to the proximity of the surface and yaw effects. Further, in Fig. 5.1, the pressure gradient in the radial direction given by the flat static probe readings is negative whereas the disc probe readings give a positive gradient. From the equation for radial equilibrium,

$$\frac{\partial P}{\partial r} = \frac{\rho U^2}{r}, \qquad \ldots(5.1)$$

we see that for convex curvature, the gradient $\frac{\partial P}{\partial r}$ is positive. Hence the readings obtained with the disc probe are considered to be more reliable. In Fig. 5.2 are given the radial pressure distributions at all different stations along the jet. It was found that the static pressure distribution across the jet did not change with surface speed in the range measured.

5.2.2 VELOCITY PROFILES

The velocity profiles measured are shown in Figs. 5.3 to 5.8. As long as the maximum jet velocity is larger than the surface speed, the velocity profiles have the familiar shape of a wall jet except for the conditions at the wall. When the maximum velocity of the jet becomes a constant equal to the surface speed, the inner and outer layer can no longer be separated as in the zero speed case. Further, it is apparent that similarity of velocity profiles does not exist over the entire length of the jet.

The effect of surface motion on the velocity profiles at $\theta = 75^\circ$ is shown in Fig. 5.9. With surface speed, the maximum jet velocity increases and the thickness of the inner layer decreases slightly. As y increases, the effect of rotation on the velocity profiles diminishes.

The non - dimensional velocity profiles for N = 800 are given in Fig. 5.10. It can be stated that similarity of velocity profiles is no longer present at all downstream positions but only exists approximately when the maximum velocity of the jet exceeds the surface speed.

The non - dimensional velocity profiles are obtained by using Um and $y_{m/2}$ as velocity and length scale respectively. Both Um and $y_{m/2}$ are functions of x in the case of no rotation whereas with rotation Um becomes a constant equal to Us after a certain distance downstream. Therefore no suitable velocity and length scale could be determined in the region of the jet where Um = Us. For this reason, the entire jet has been broken up into three regions:

(a) Region I is the potential core region.
$(0^\circ \leq \theta \leq 15^\circ)$

(b) Region II is the mixing region with maximum velocity decay.

(c) Region III is the mixing region with constant Um = Us.

Only in Region II are the velocity profiles approximately similar and the maximum velocity decay and jet growth rates comparable to the case of no rotation. Non -

dimensional velocity profiles in Region II for other speeds are shown in Figs. 5.11 to 5.15. Fig. 5.15 contains only results of 3 stations to avoid overcrowding.

5.2.3 MAXIMUM VELOCITY DECAY AND JET GROWTH

The maximum velocity decay can be seen in Fig. 5.16 and 5.17. When the surface speed is low (N = 350), the maximum velocity decay is only slightly affected and follows the familiar trend of the zero speed case. This type of velocity decay is observed in Region II at the other surface speeds with a slight increase in Um but no appreciable effect on the rate of decay. In Region III, the plots in Figs. 5.16 and 5.17 indicate a marked difference from the zero rotation case. This deviation is more due to the difficulty in the treatment of the data because of the lack of a suitable velocity scale than actual physical conditions.

The plots of the maximum velocity coefficient in Region III of Fig. 5.17 have a positive slope. However, this should not be interpreted as a velocity increase. Actually, Um in Region III is a constant equal to Us.

Figure 5.18, obtained with the help of Fig. 5.16, shows that the upper limit of Region II, θ_2, decreases with an increase of the surface speed. The experimental mean line is extrapolated to the point defined by Us/Uo = 1.0 and $\theta_2 = 0$ because Region II vanishes when Us = Uo.

The jet growth is shown in Fig. 5.19. For X^1 less than about 40, the rate of jet growth seems to be unaffected by N. For X^1 larger than about 40, the rates are markedly

different from the zero speed case even at the low surface speed (N = 350). For higher speeds, the deviations are primarily due to the lack of a suitable length scale.

5.2.4 OPPOSITE ROTATION

The velocity profiles obtained with the surface spinning (N = 500) in the direction opposite to the jet flow are given in Fig.5.20. A comparison of Fig. 5.20 and Fig. 5.3 shows that Um is decreased and $y_{m/2}$ is increased at each downstream station in the case of opposite rotation. This is more clearly seen in Figs. 5.16 and 5.19. The effects of rotation on Um and $y_{m/2}$ are more appreciable in the case of opposite rotation than direct rotation.

5.2.5 SEPARATION

For N = 0, θ_{sep} is found to be 205 degrees. Fekete (Ref. 4) found θ_{sep} to be 210 degrees for Re > 4×10^4 with some dependence on the roughness of the surface, θ_{sep} decreasing with an increase of roughness. Therefore the present value of 205 degrees is considered satisfactory.

The variation of the angular position of separation θ_{sep} with the surface speed is shown in Fig 5.21. It should be pointed out that separation in the case of a rotating cylinder means separation of the jet from the boundary layer flow over the cylinder.

For positive Us/Uo, θ_{sep} initially increases with Us/Uo (or N) but remains constant at 245 degrees for values larger than 0.2.

With opposite rotation, θ_{sep}. decreases almost

linearly with -Us/Uo. At Us/Uo = -0.53, $\theta_{sep} = 0$, i.e., no jet attachment. This value is obtained by extrapolating the experimental mean line (shown dotted).

CHAPTER VI

CONCLUSIONS

1. Similarity of velocity profiles does not exist over the entire length of the jet.

2. There are three regions of jet flow:

   Region I - potential core region

   Region II - mixing region with maximum velocity decay

   Region III - mixing region with constant Um

3. In Region II, the velocity profiles are approximately similar and the rates of jet growth and maximum velocity decay are not appreciably affected by rotation.

4. In Region III no suitable length and velocity scale could be determined.

5. The radial static pressure distribution across the jet is linear and unaffected by rotation within the range of the experiments.

6. With the surface spinning in the direction of the jet, θ_{sep} initially increases with N and reaches a constant

value of 245 degrees.

7. In the case of opposite rotation, $\theta_{sep.}$ decreases linearly with N.

LIST OF REFERENCES

1. Glauert, M. B. The Wall Jet, J. Fluid Mech., Volume 1, P. 625. (1956).

2. Newman, B. G. The Deflection of Plane Jets by Adjacent Boundaries - Coanda Effect. Boundary Layer and Flow Control, Vol. 1, Edited by G. V. Lachman, Pergamon Press, P. 232, (1961).

3. Nakaguchi, H. Jet Along a Curved Wall. Dept. of Aeronautics, University of Tokyo, Research Memo No. 4. (1961).

4. Fekete, G. I. Coanda Flow of a Two Dimensional Wall Jet on the Outside of a Circular Cylinder. McGill University, Report No. 63 - 11. (1963).

5. Rarity, B. S. H. The Wall Jet on a Rotating Disc, Quart. Journal, Mech, and Applied Math., Vol.XVIII Pt. 4, P. 4. (1965).

6. Schwarz, W. H. Cosart, W. P. Two - Dimensional Turbulent Wall Jet. J. Fluid Mech., Vol. 10, Pt. 4, P481. (1961).

7. Myers, G. E. Schauer, J. J. Eustis, R. N. Plane Turbulent Wall Jet. Part 1, Dept. of Mechanical Engineering, Stanford University, Tech. Report NO. 1. (1961).

8. Sigalla, A. Measurements of Skin Friction in a Plane Turbulent Wall Jet, J. Roy. Aero. Soc., 62 P873. (1958).

9. Gartshore, I. Hawaleshka, O. The Design of a Two - Dimensional Blowing Slot and Its Application to a Turbulent Wall Jet in Still Air. Tech. Note 64 - 5, McGill University. (1964).

10. Neville, A. M. Kennedy, J. B. Basic Statistical Methods for Engineers and Scientists, International Text - book Co. (1964).

11. Tu, P. K. C. Thesis to be published.

TABLE 2.1

CONSTANTS FOR PLANE WALL JET

	Investigator	Probe	a	b	Power Law Exp.	Re
1	Glauert	Theory	-.517	.95	$\frac{1}{7}$	
2	Sigalla	Preston (Pitot)	-.500	1.0	$\frac{1}{7}$	6.2×10^4
3	Gartshore and Hawaleshka	Pitot	-.53	1.0	$\frac{1}{11.4}$	
4	Schwarz and Cosart	Hot Wire	-.555	1.0	$\frac{1}{14}$	2.2×10^4 Re 10.6×10^4
5	Myers, Schaver and Eustis	Total Head and Kiel	$-.49 \pm .03$	$.95 \pm .03$	$\frac{1}{14}$	

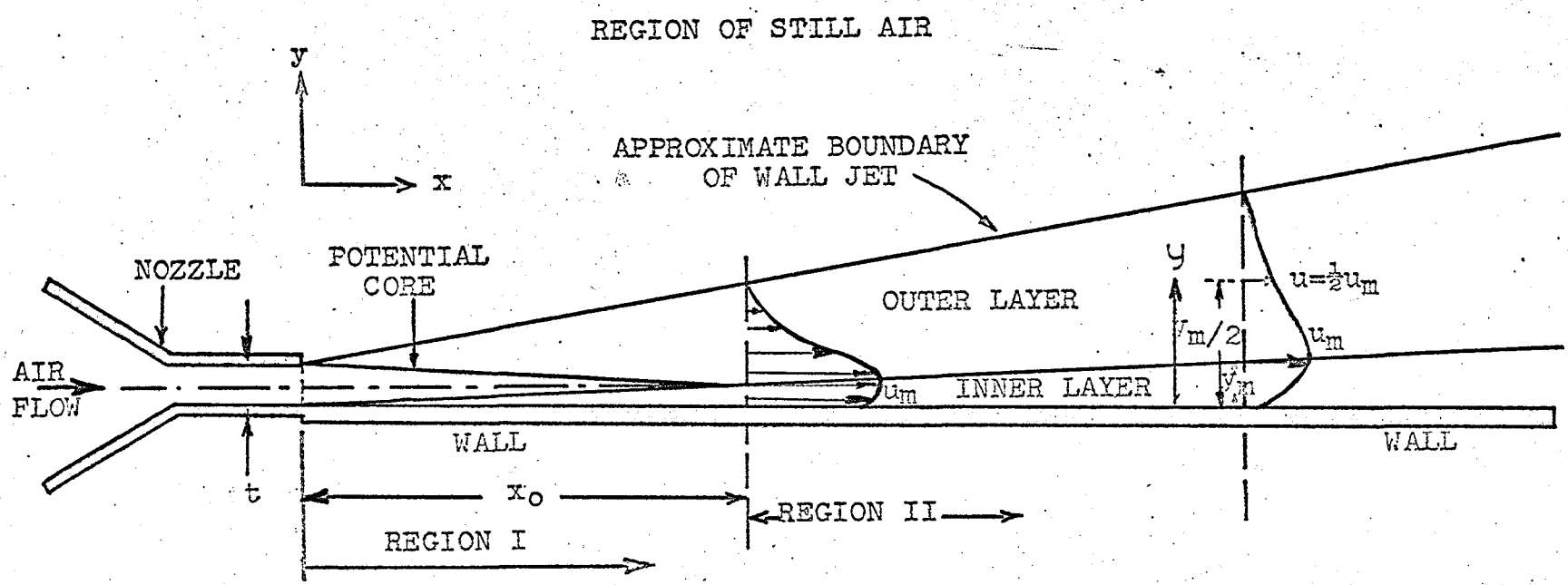

FIG. 2.1 WALL JET NOMENCLATURE

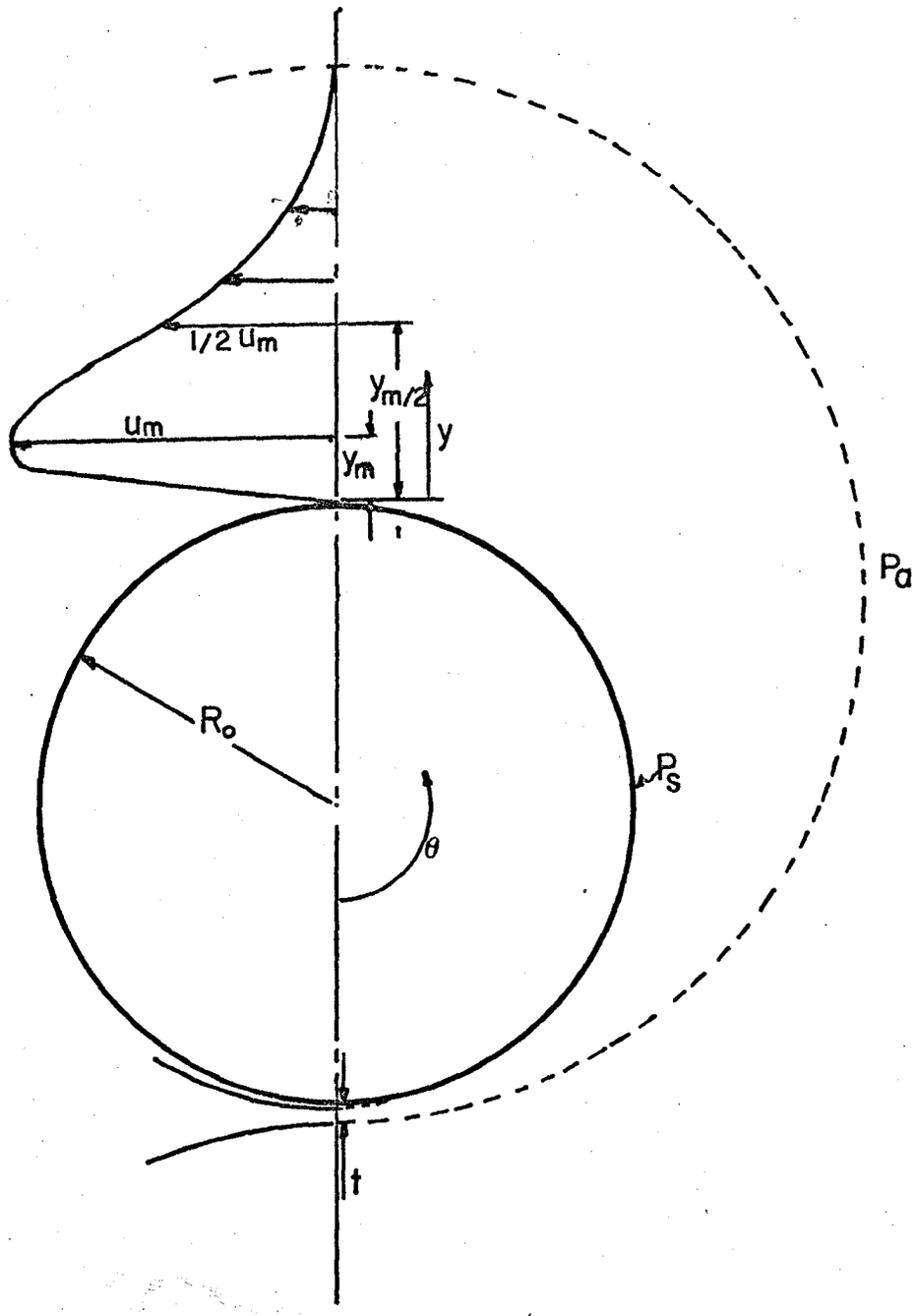

Fig. 2.2 CURVED WALL JET NOMENCLATURE

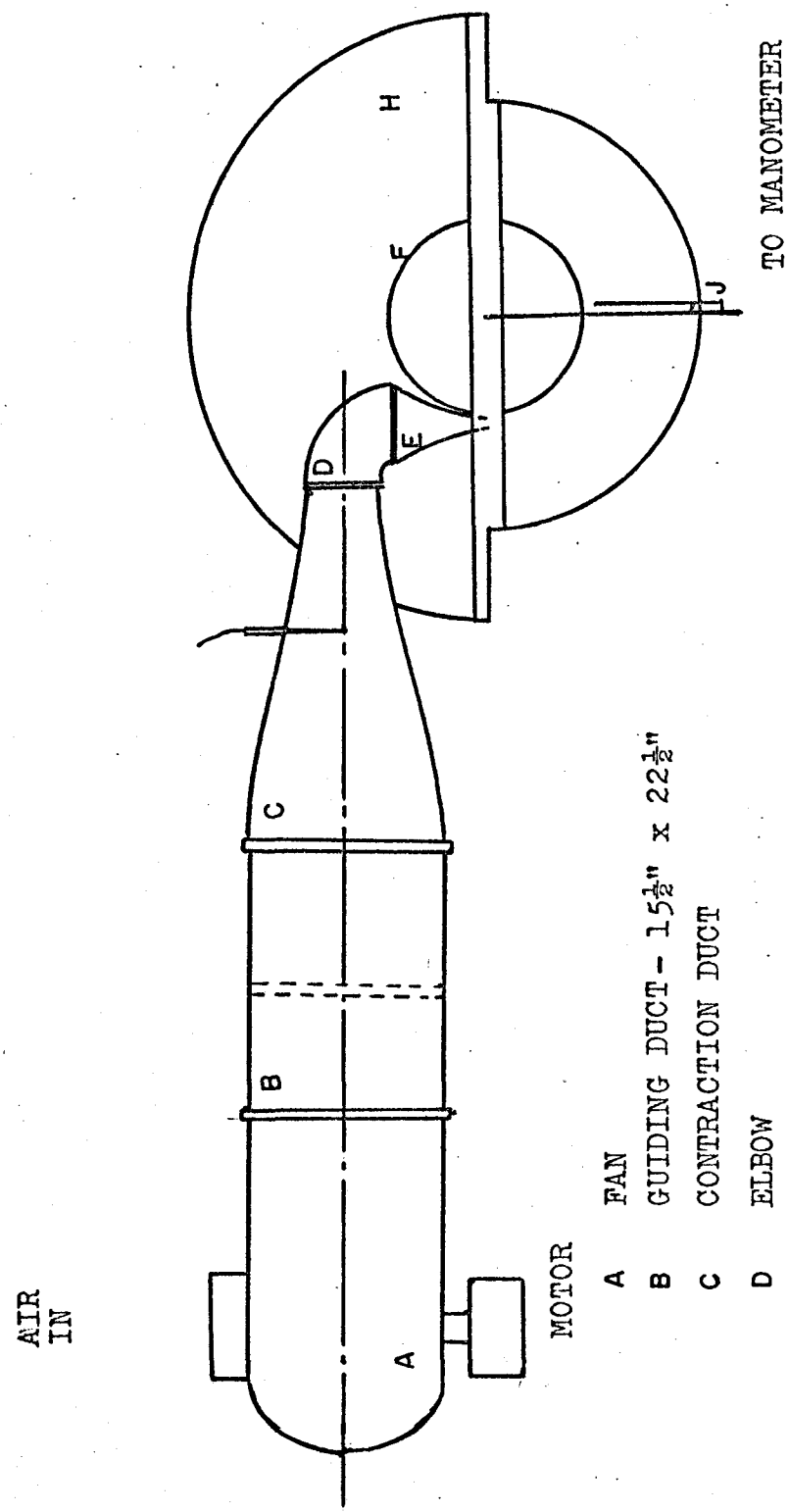

Fig. 3.1 SCHEMATIC DIAGRAM OF TEST FACILITIES

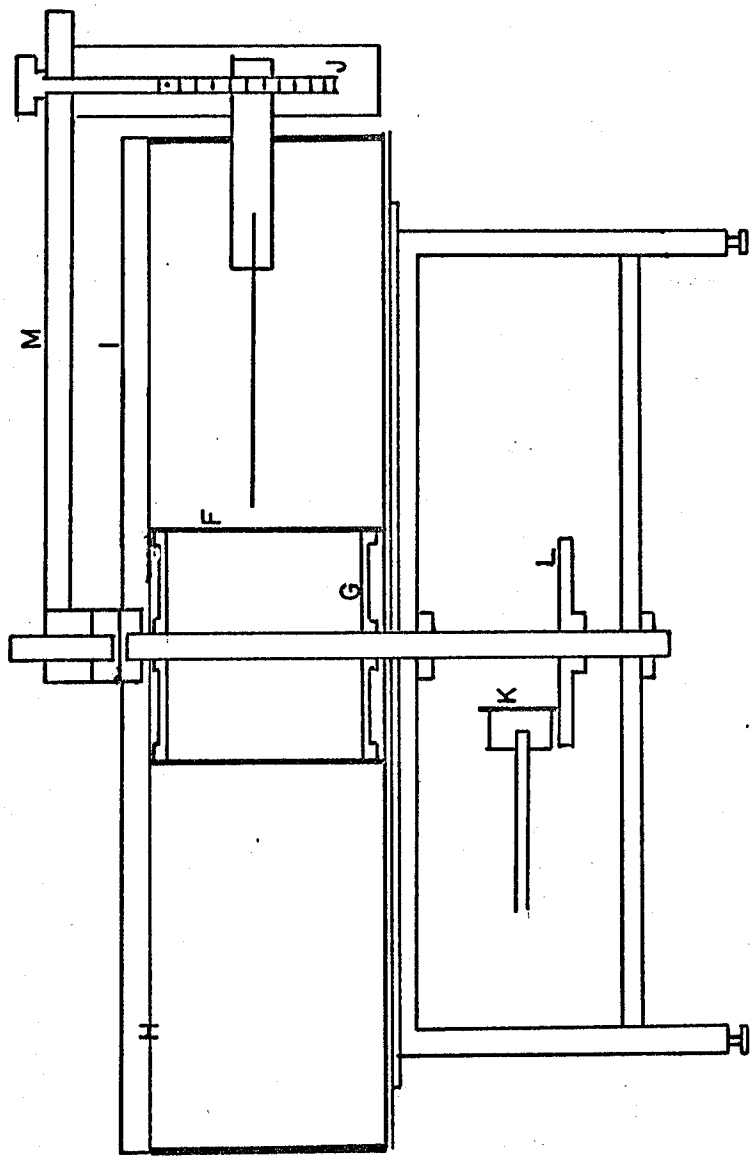

H END PLATES

I ANGLE

J TRAVERSING MECHANISM

K DRIVING WHEEL

L DRIVEN WHEEL

M TRAVERSING ARM

Fig. 3.2 SKETCH OF ROTATING CYLINDER AND DRIVE

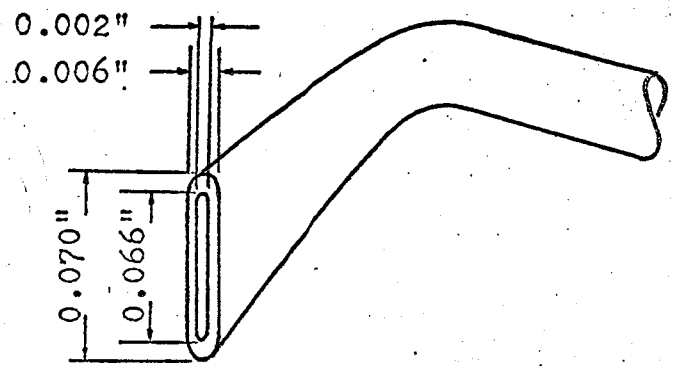

(a) TOTAL PRESSURE PROBE

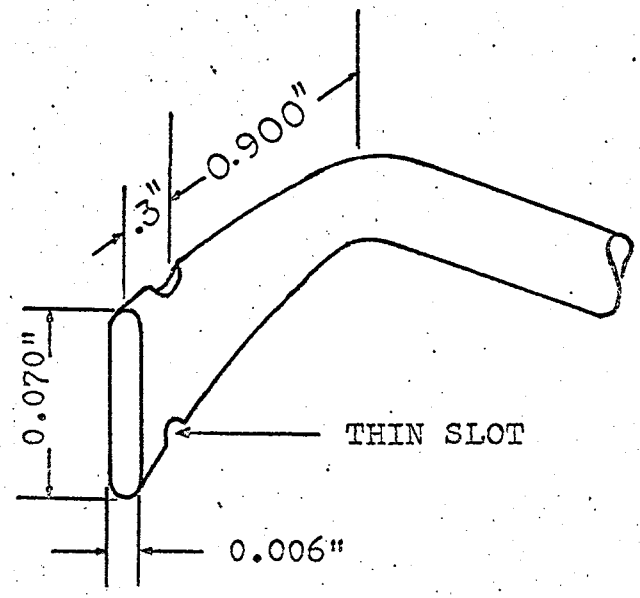

(b) STATIC PRESSURE PROBE

Figs. 3.3a,b FLAT STATIC AND TOTAL PRESSURE PROBE

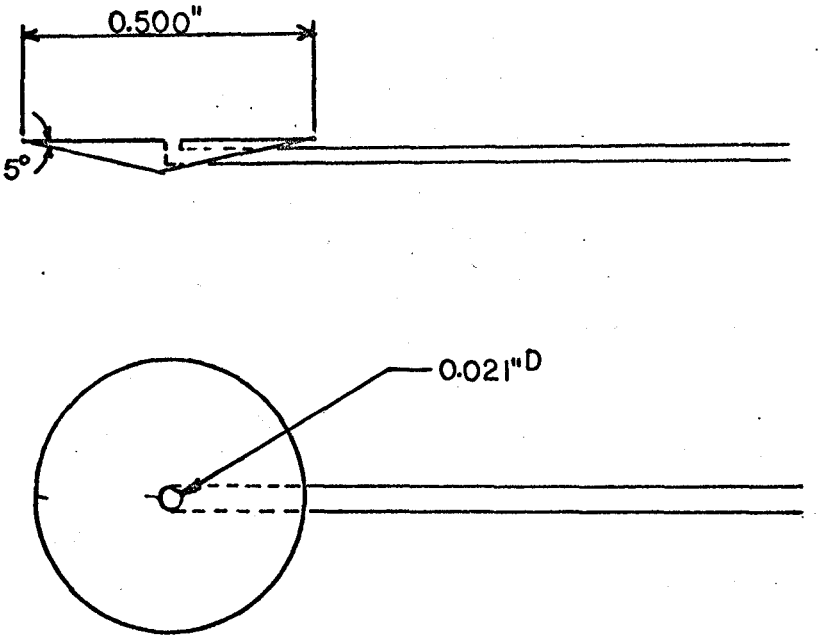

(c) DISC PROBE

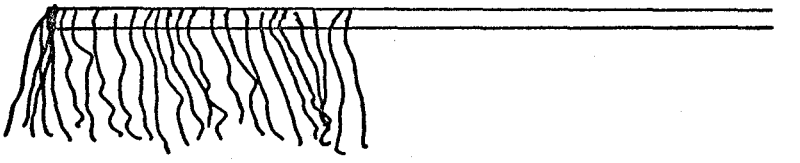

(d) TUFT PROBE

Figs. 3.3 c,d DISC AND TUFT PROBES

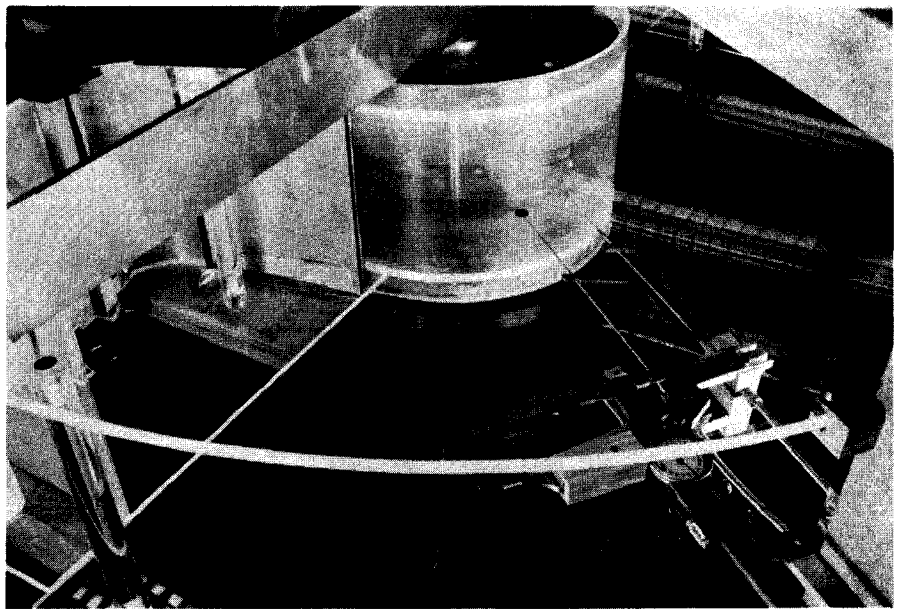

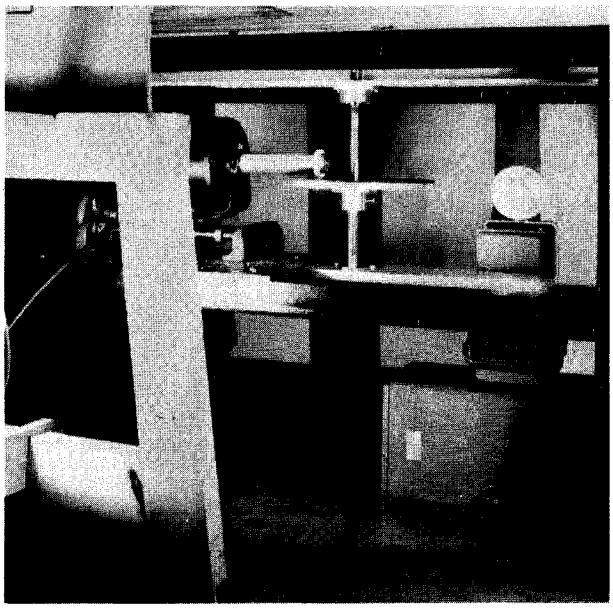

Fig. 3.4 VIEW OF EXPERIMENTAL ARRANGEMENT

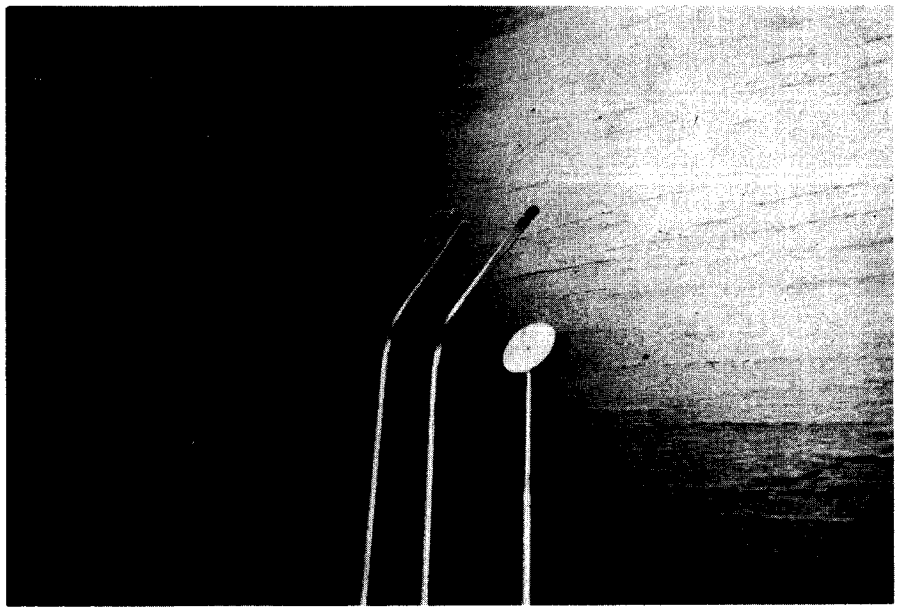

Fig. 3.5 VIEW OF PRESSURE PROBES

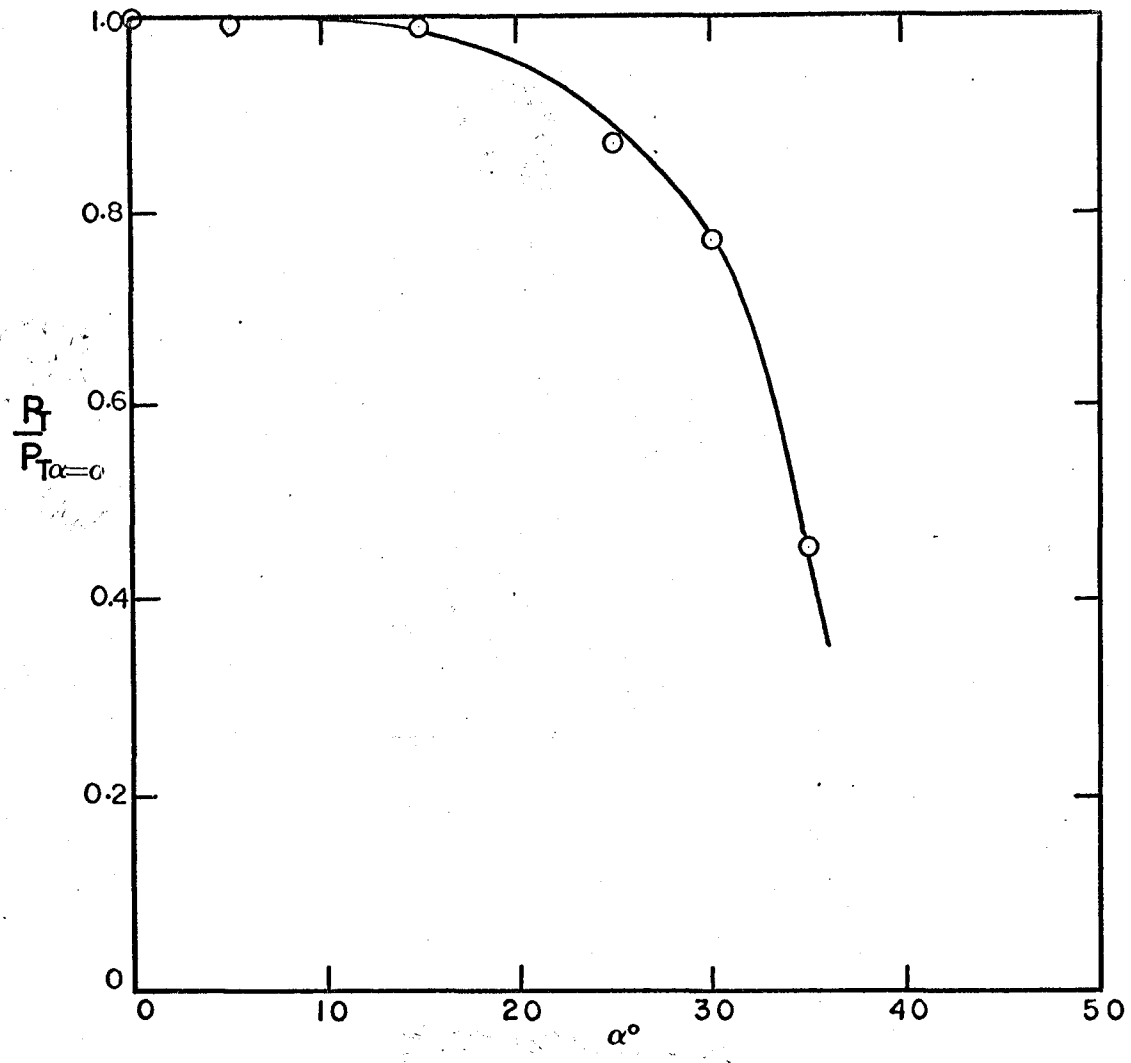

Fig. 4.1 YAW CALIBRATION OF FLAT TOTAL PRESSURE PROBE

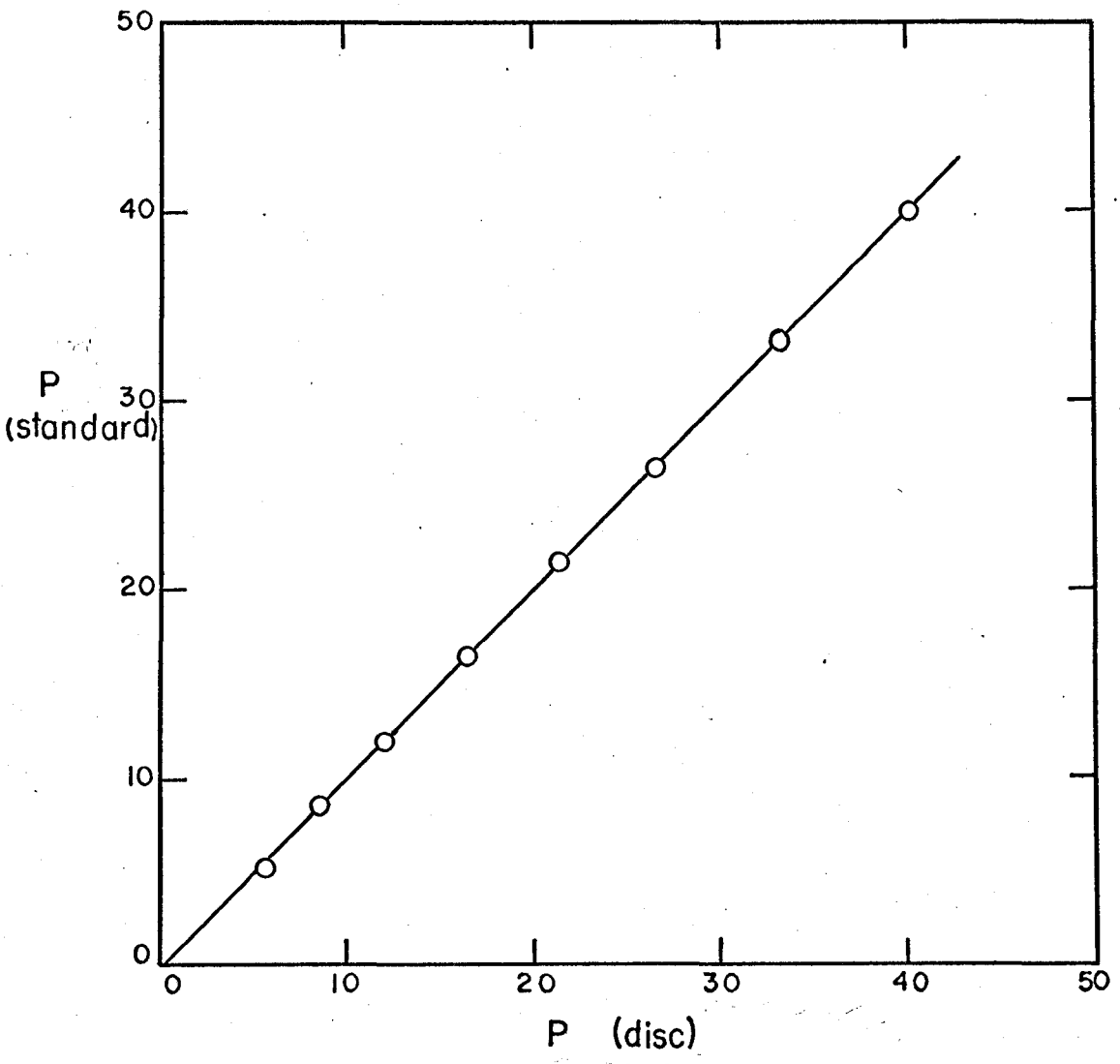

Fig. 4.2 CALIBRATION OF DISC PROBE

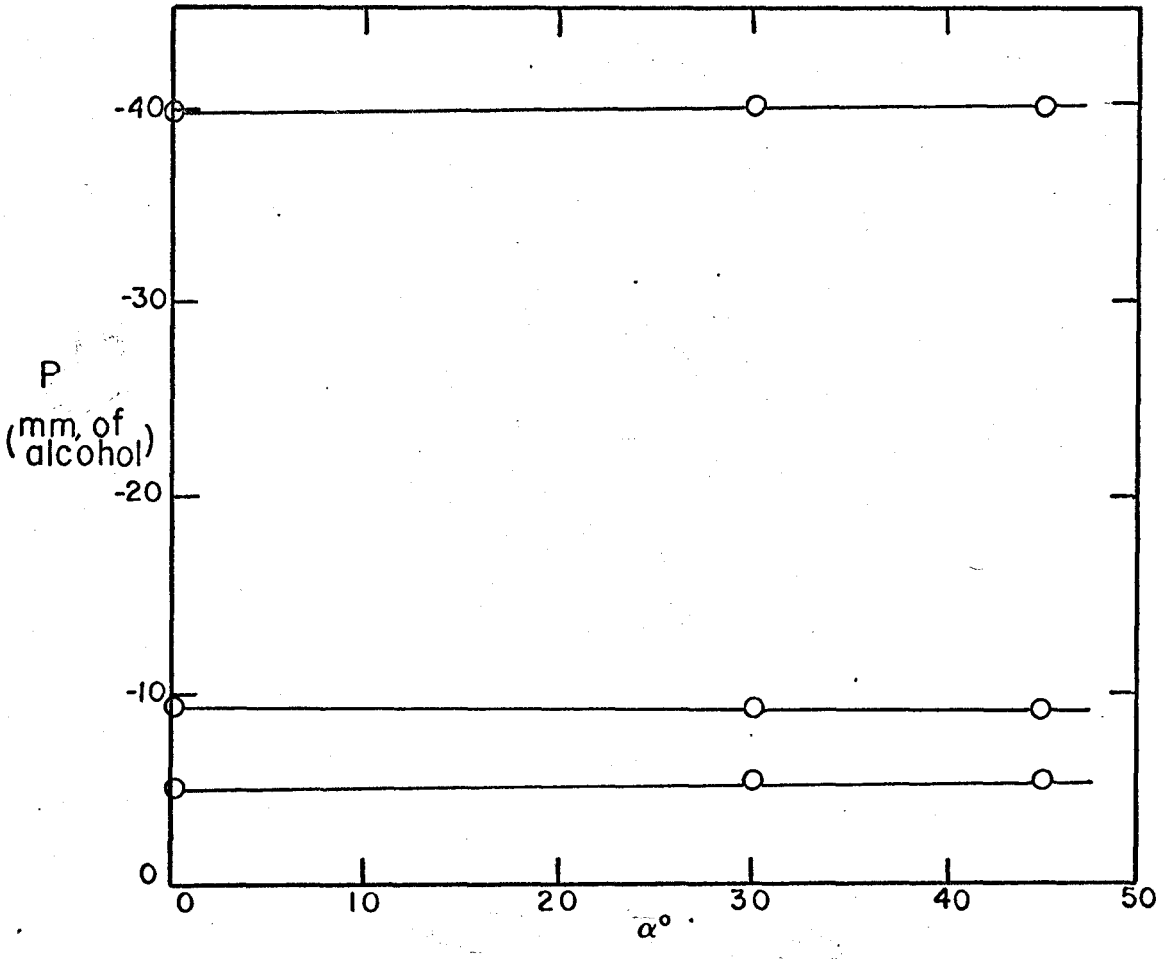

Fig. 4.3 YAW CALIBRATION OF DISC PROBE

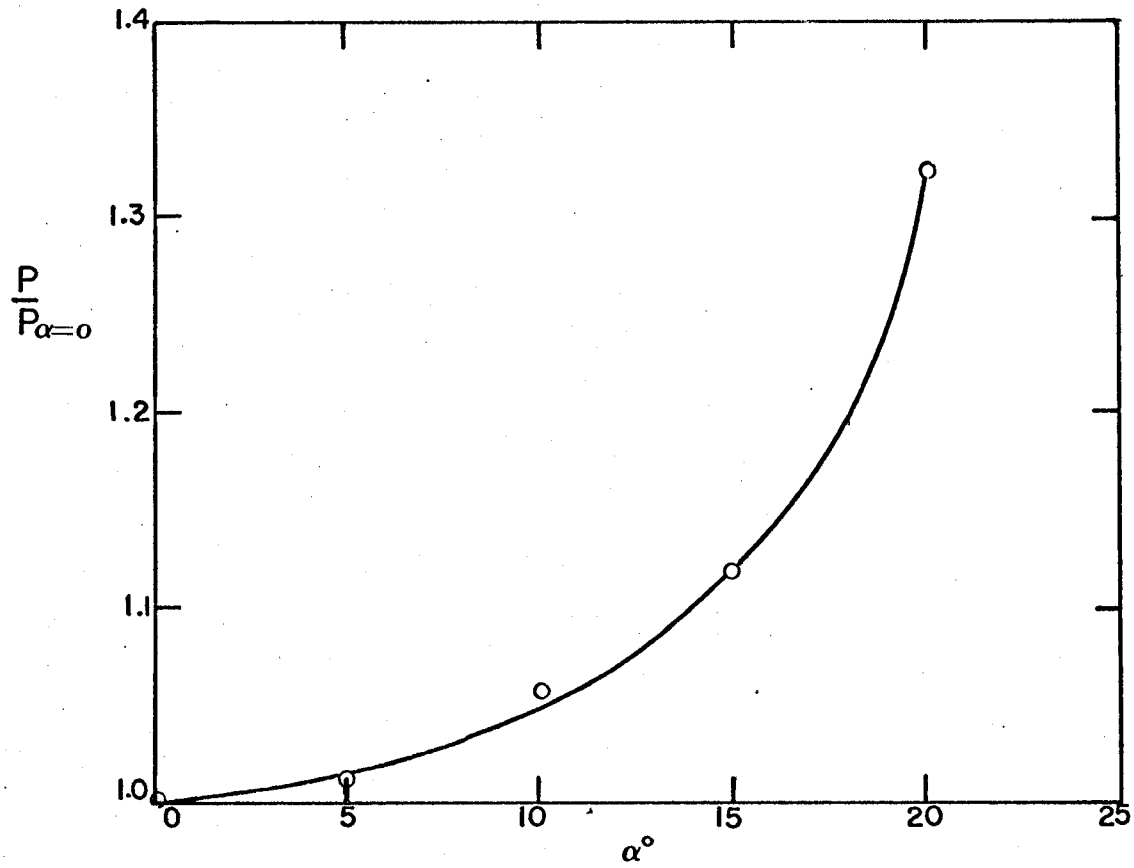

Fig. 4.4 YAW CALIBRATION OF FLAT STATIC PROBE

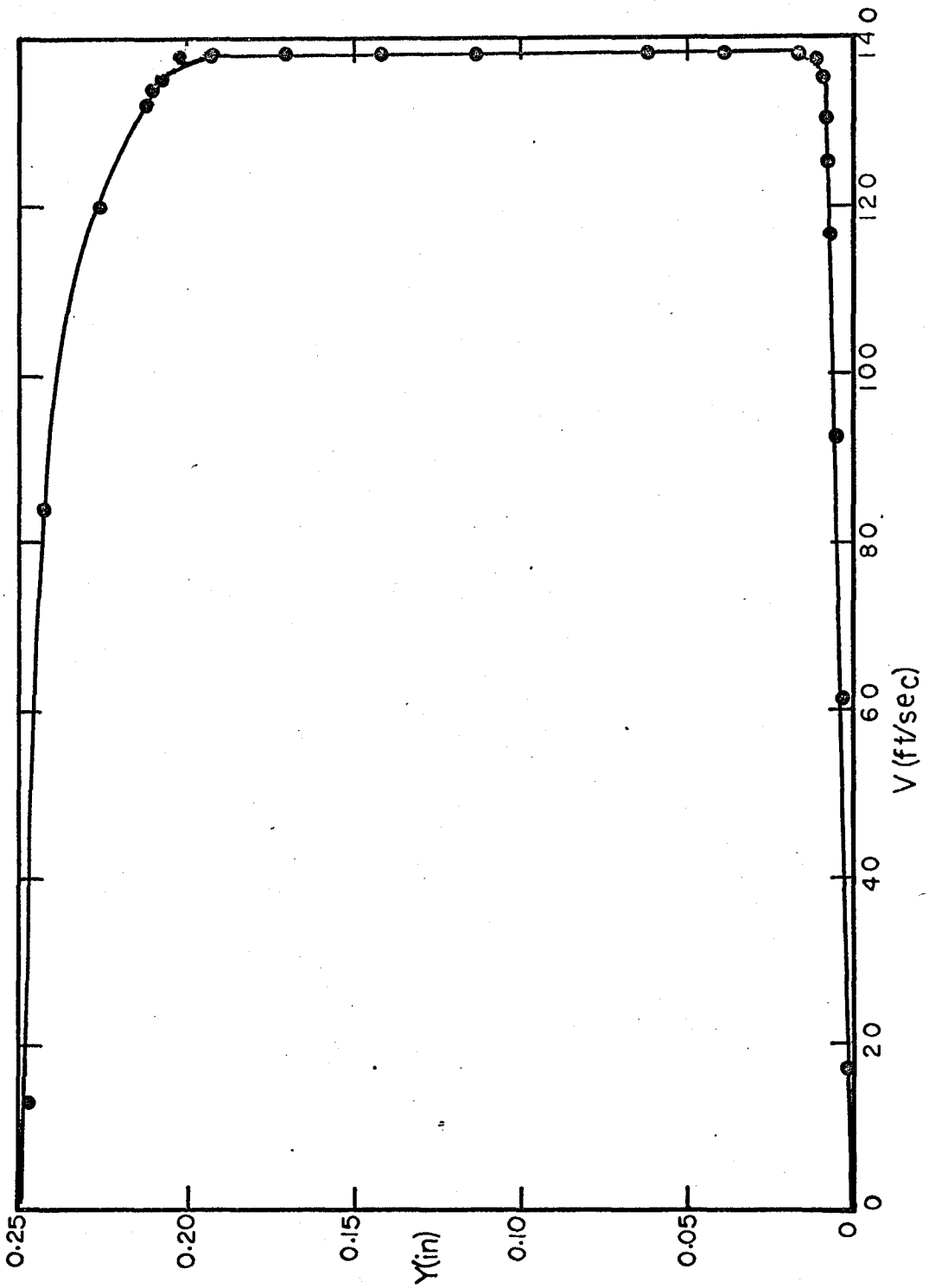

Fig. 4.5 VELOCITY PROFILE OF NOZZLE AT MID-SPAN

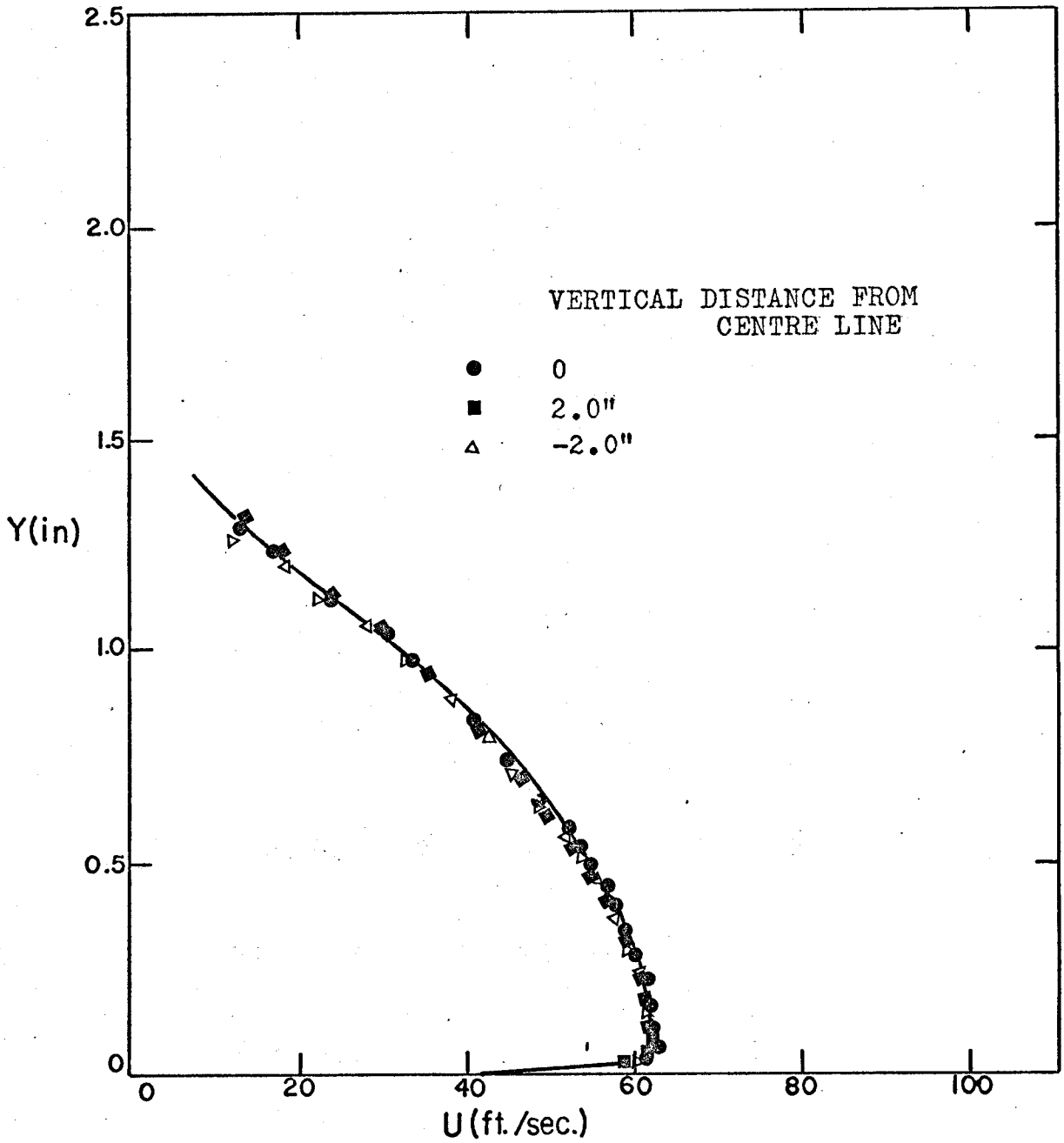

Fig. 4.6 TWO DIMENSIONALITY CHECK

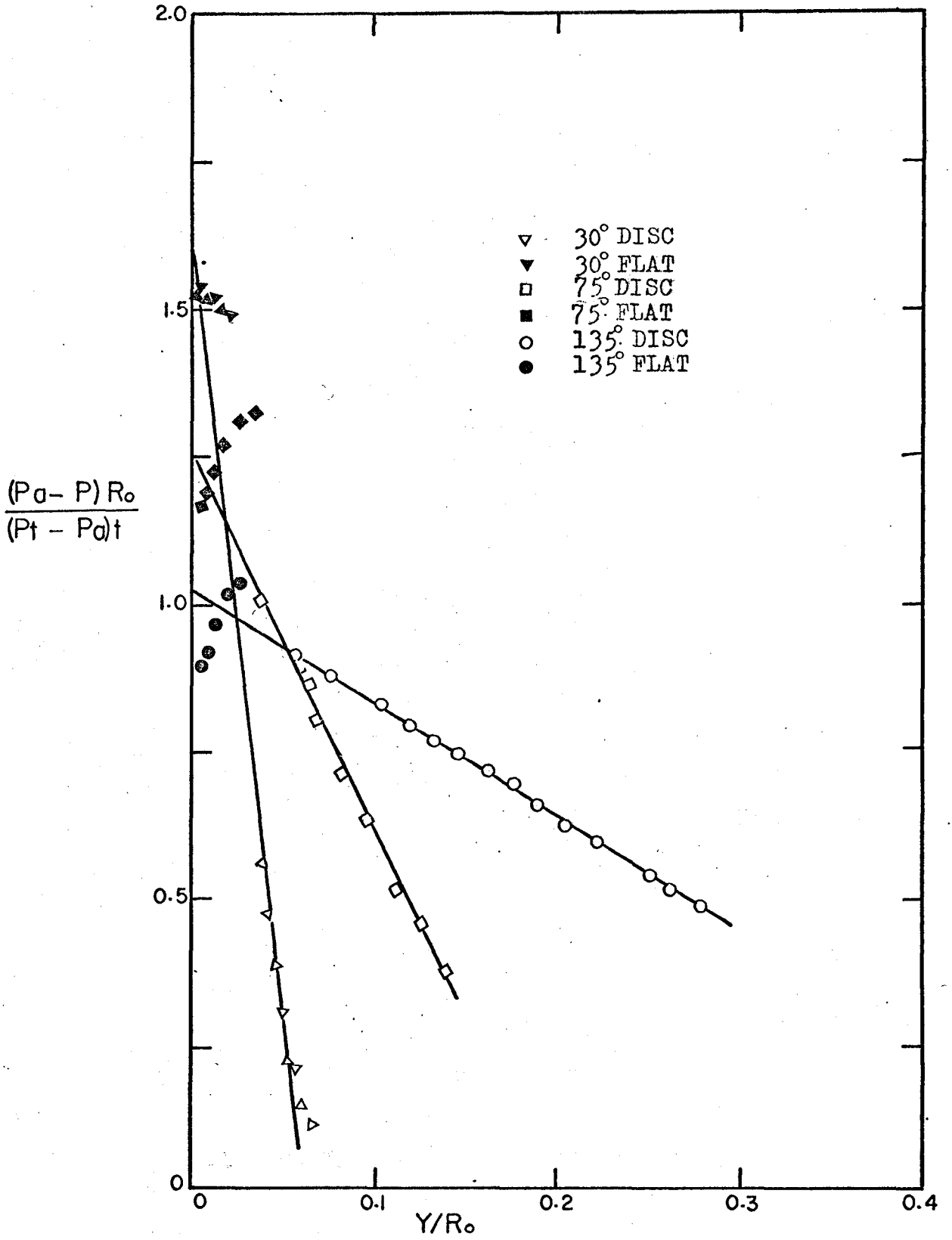

Fig. 5.1 RADIAL STATIC PRESSURE DISTRIBUTIONS

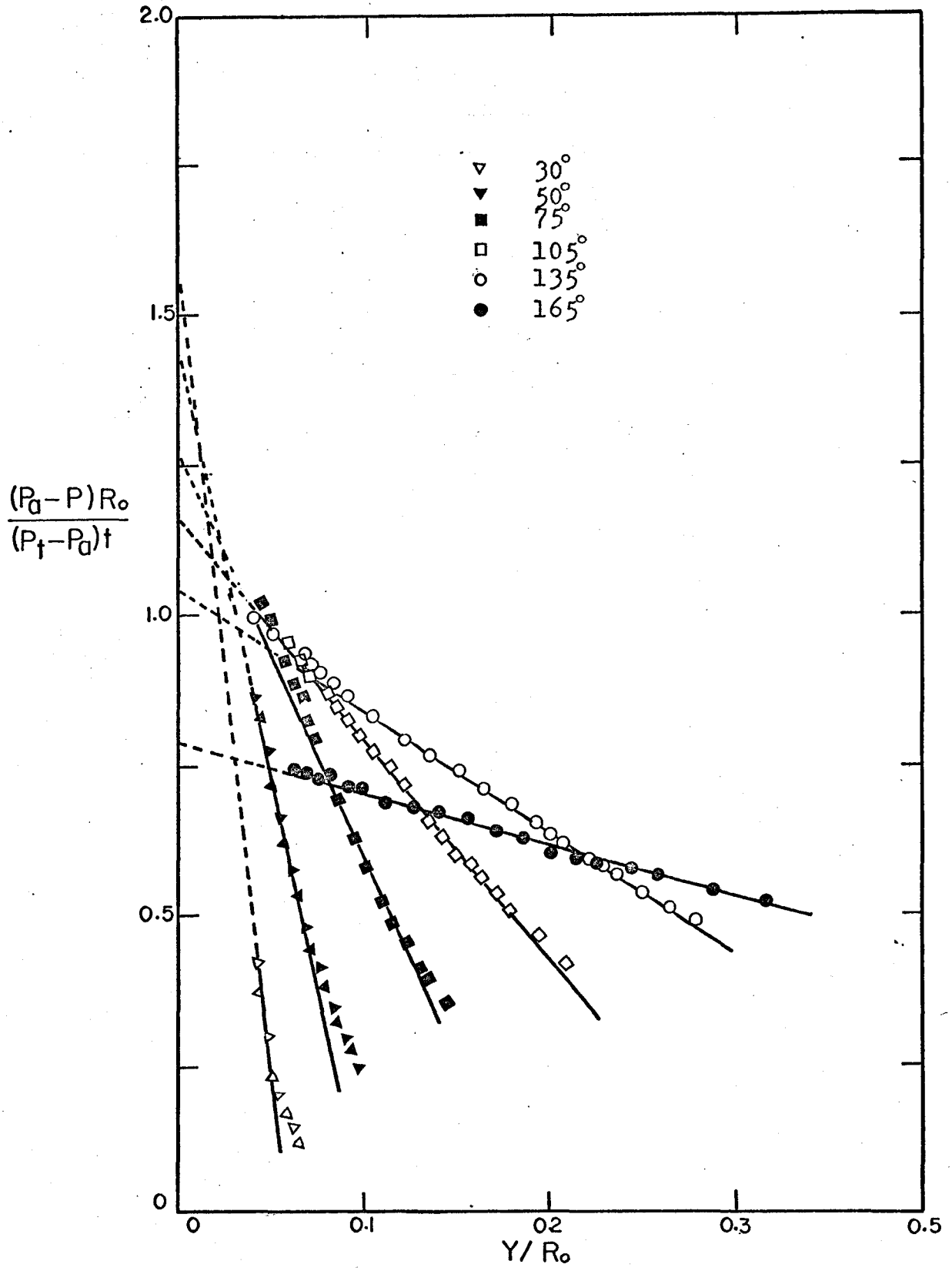

Fig. 5.2 RADIAL STATIC PRESSURE DISTRIBUTIONS OBTAINED WITH DISC PROBE

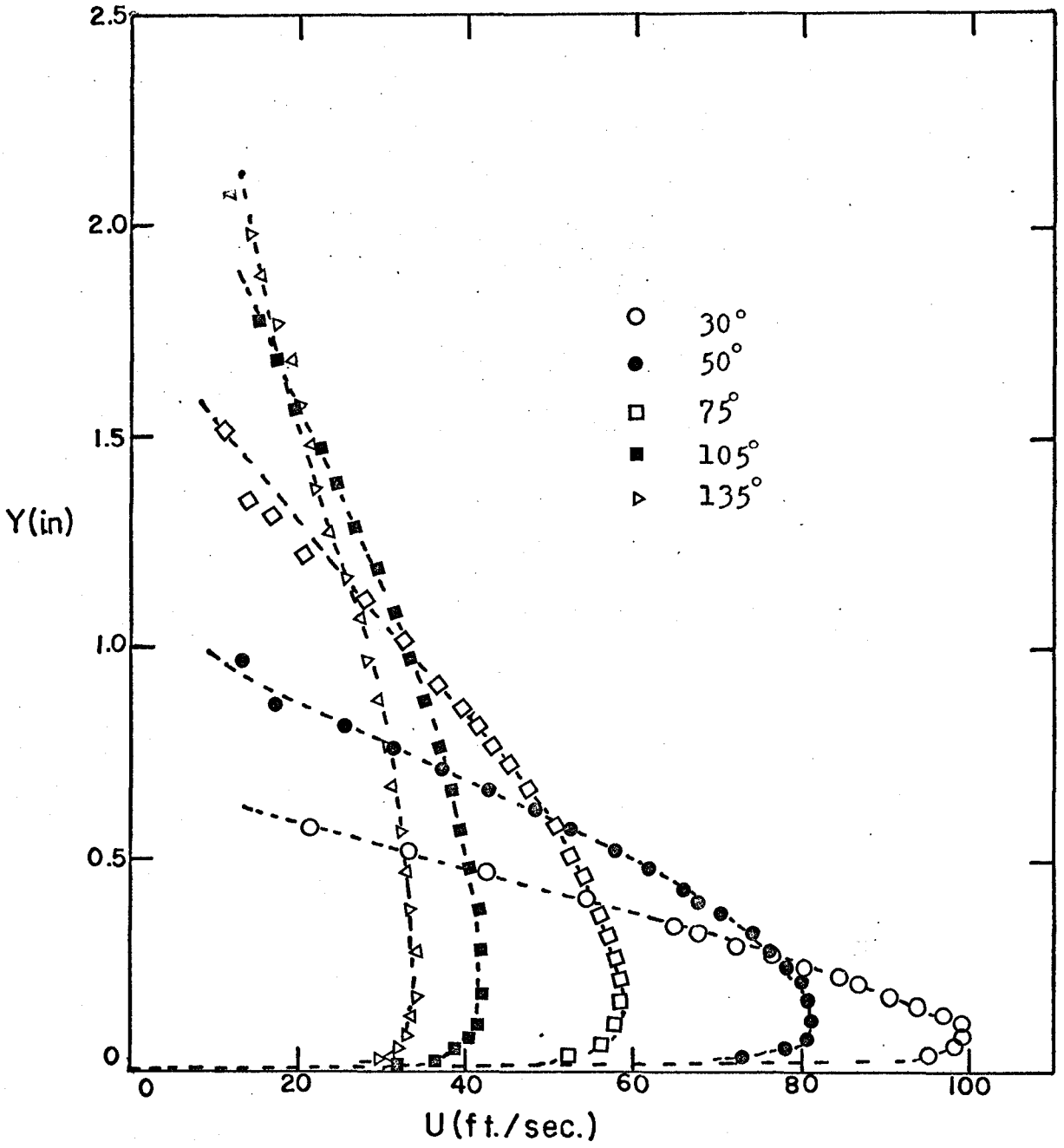

Fig. 5.3 DIMENSIONAL VELOCITY PROFILES (N = 0)

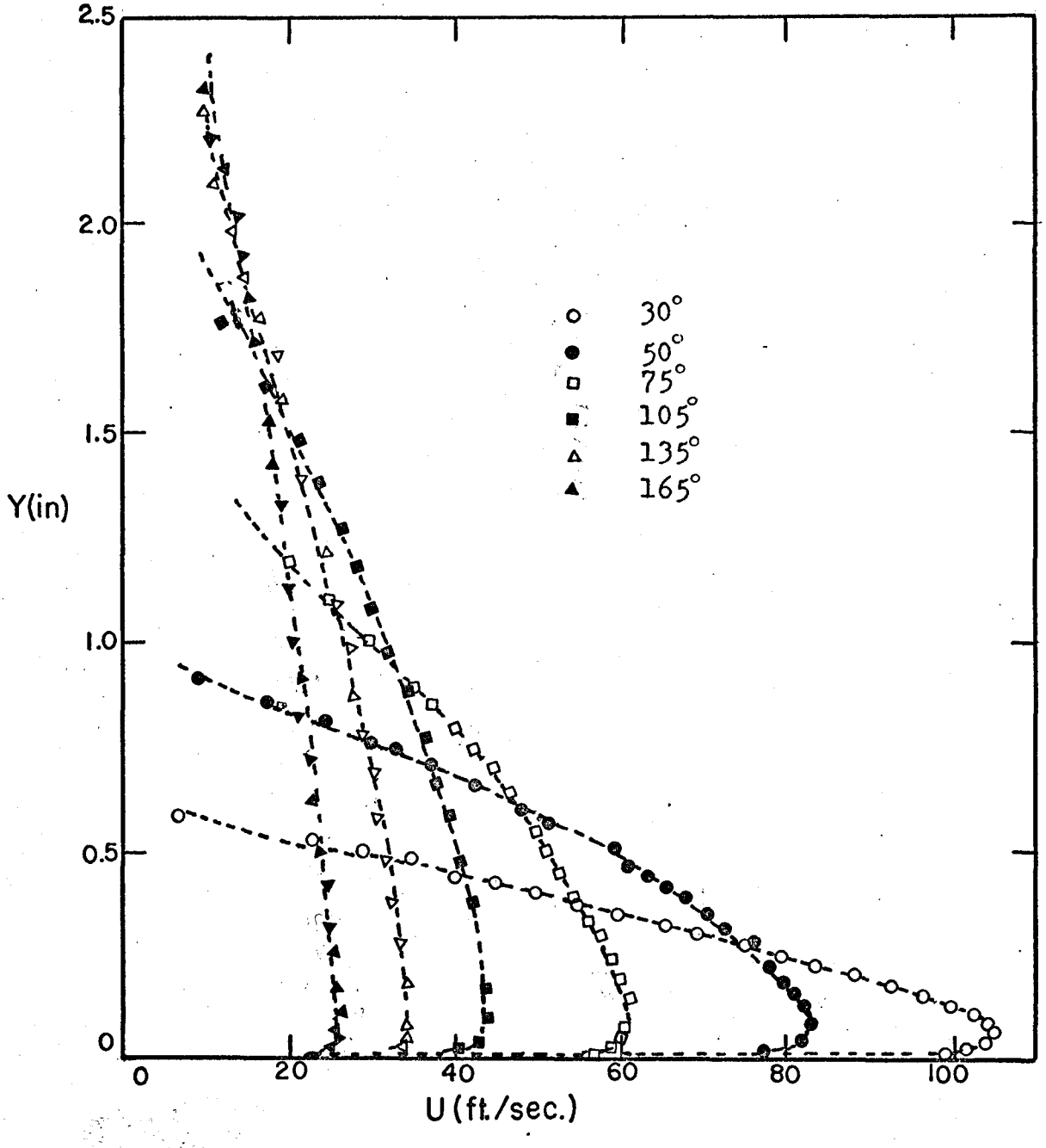

Fig. 5.4 DIMENSIONAL VELOCITY PROFILES (N = 350)

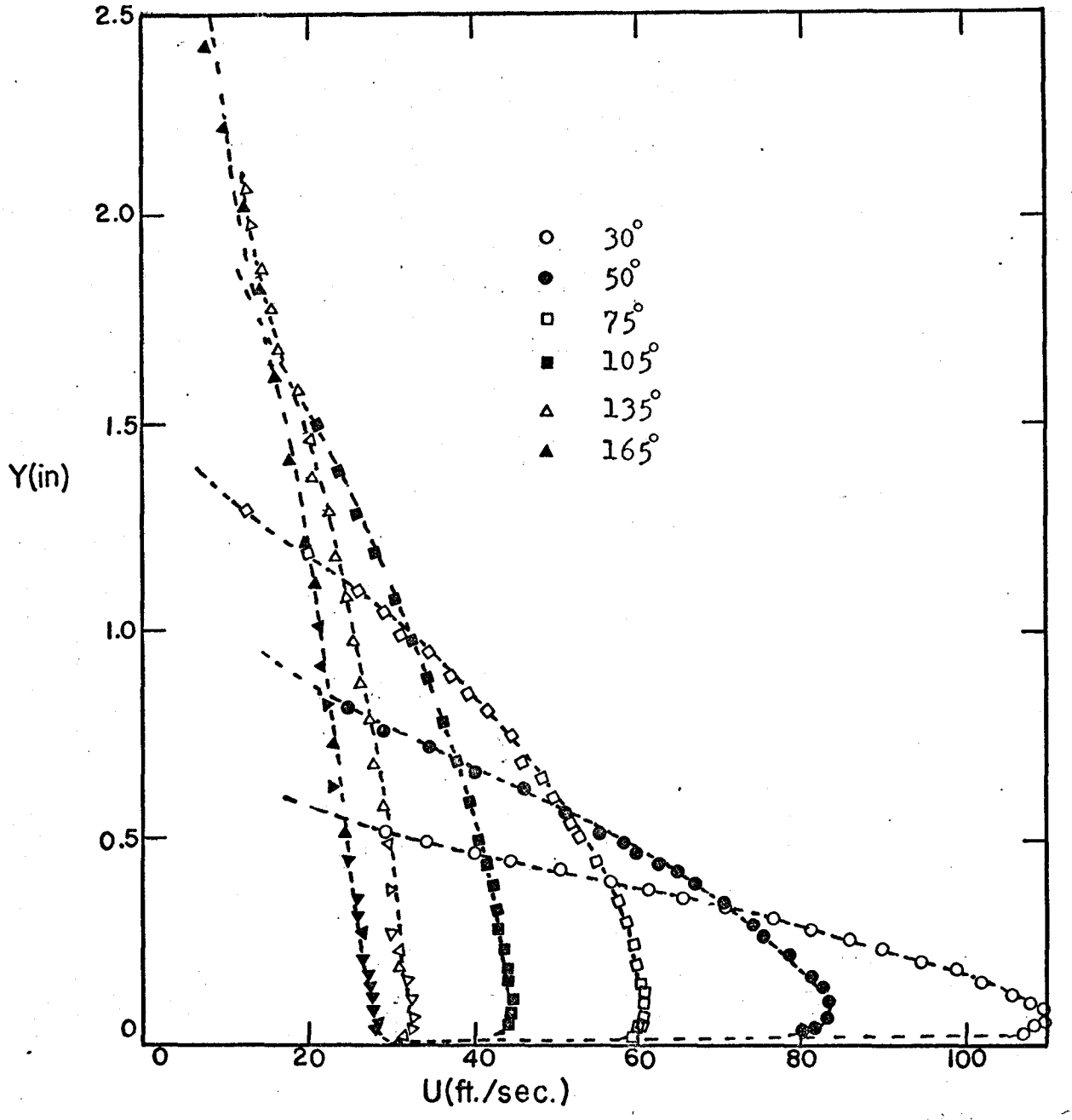

Fig. 5.5 DIMENSIONAL VELOCITY PROFILES (N = 500)

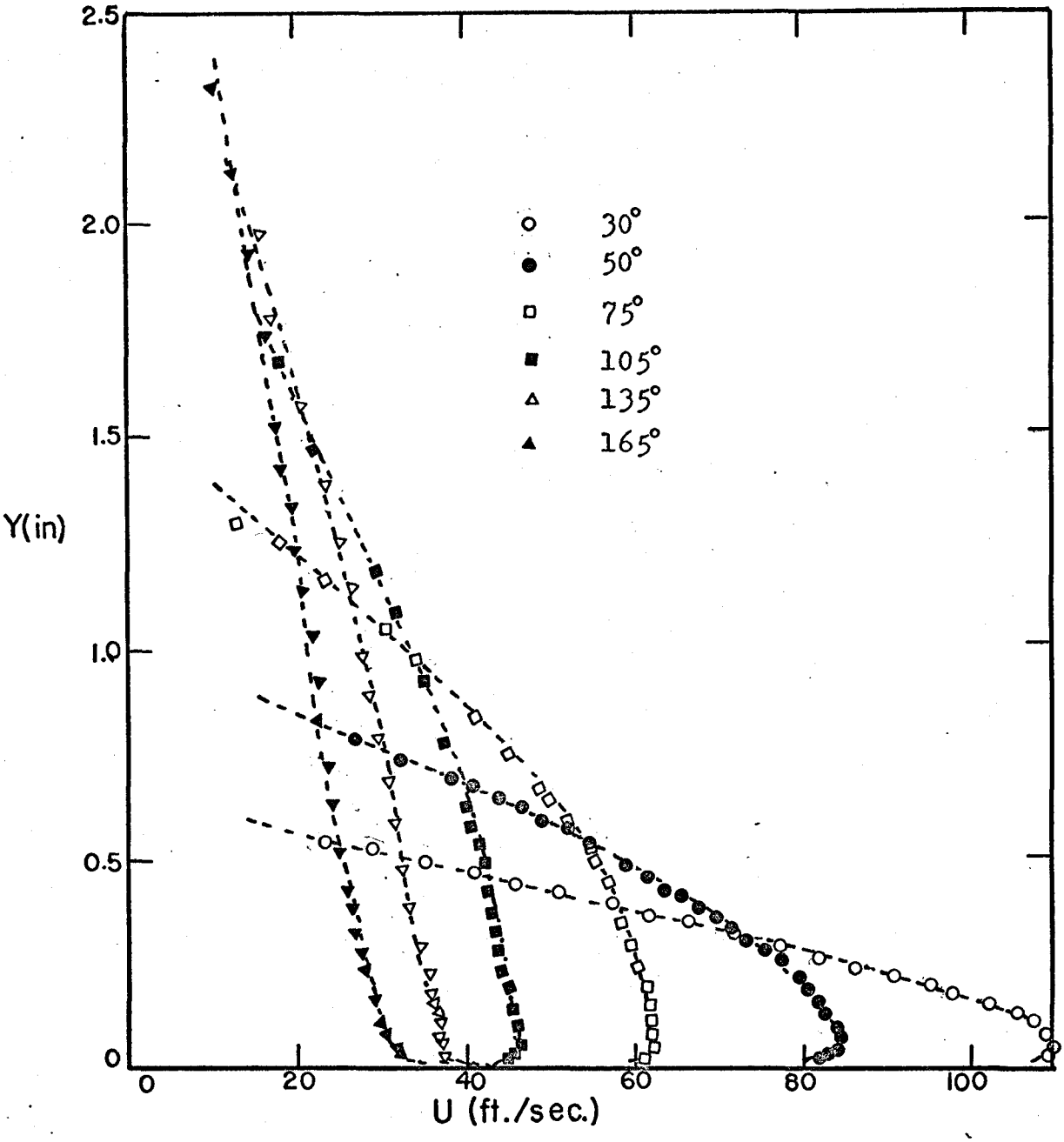

Fig. 5.6 DIMENSIONAL VELOCITY PROFILES (N = 700)

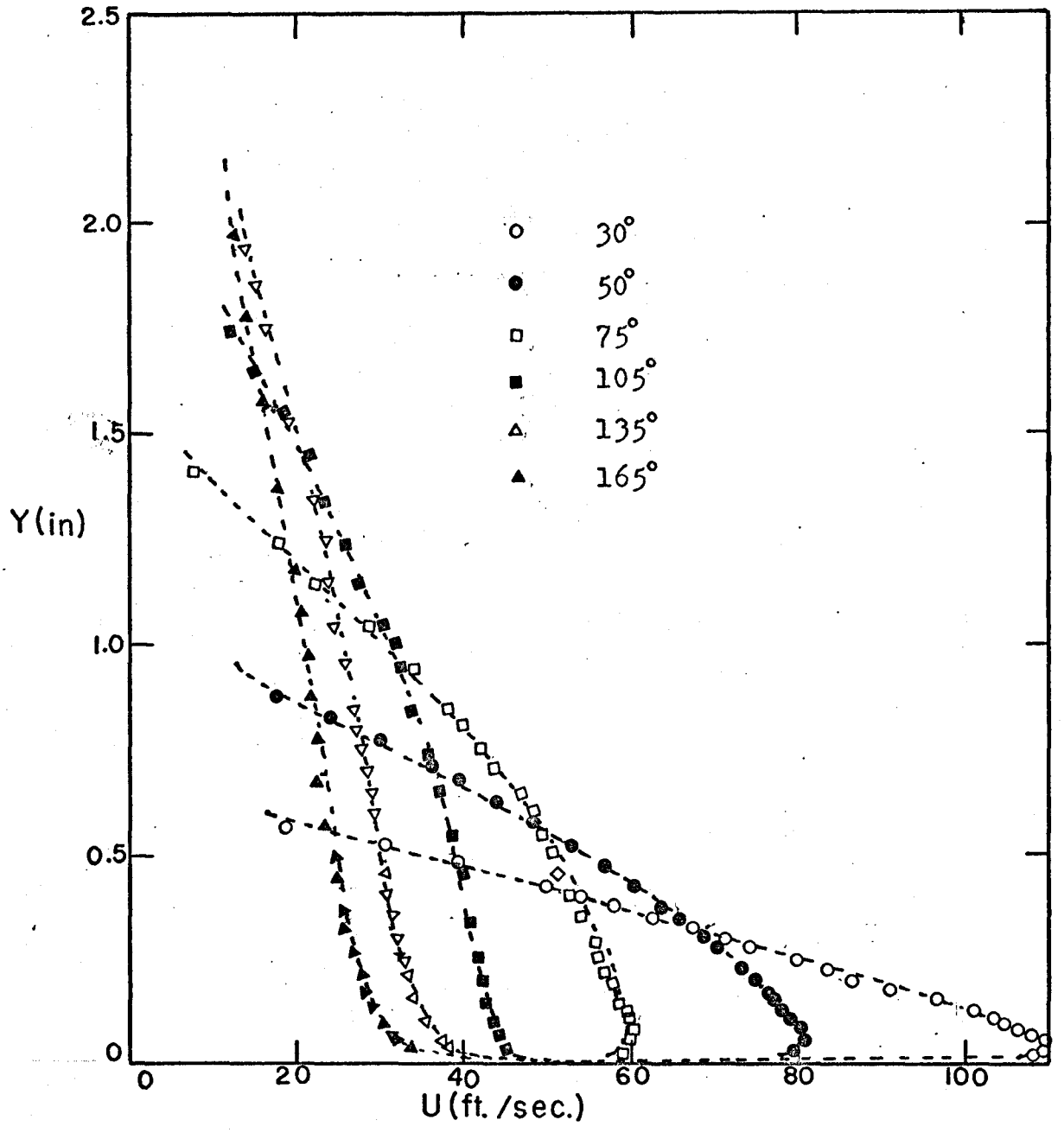

Fig. 5.7 DIMENSIONAL VELOCITY PROFILES (N = 800)

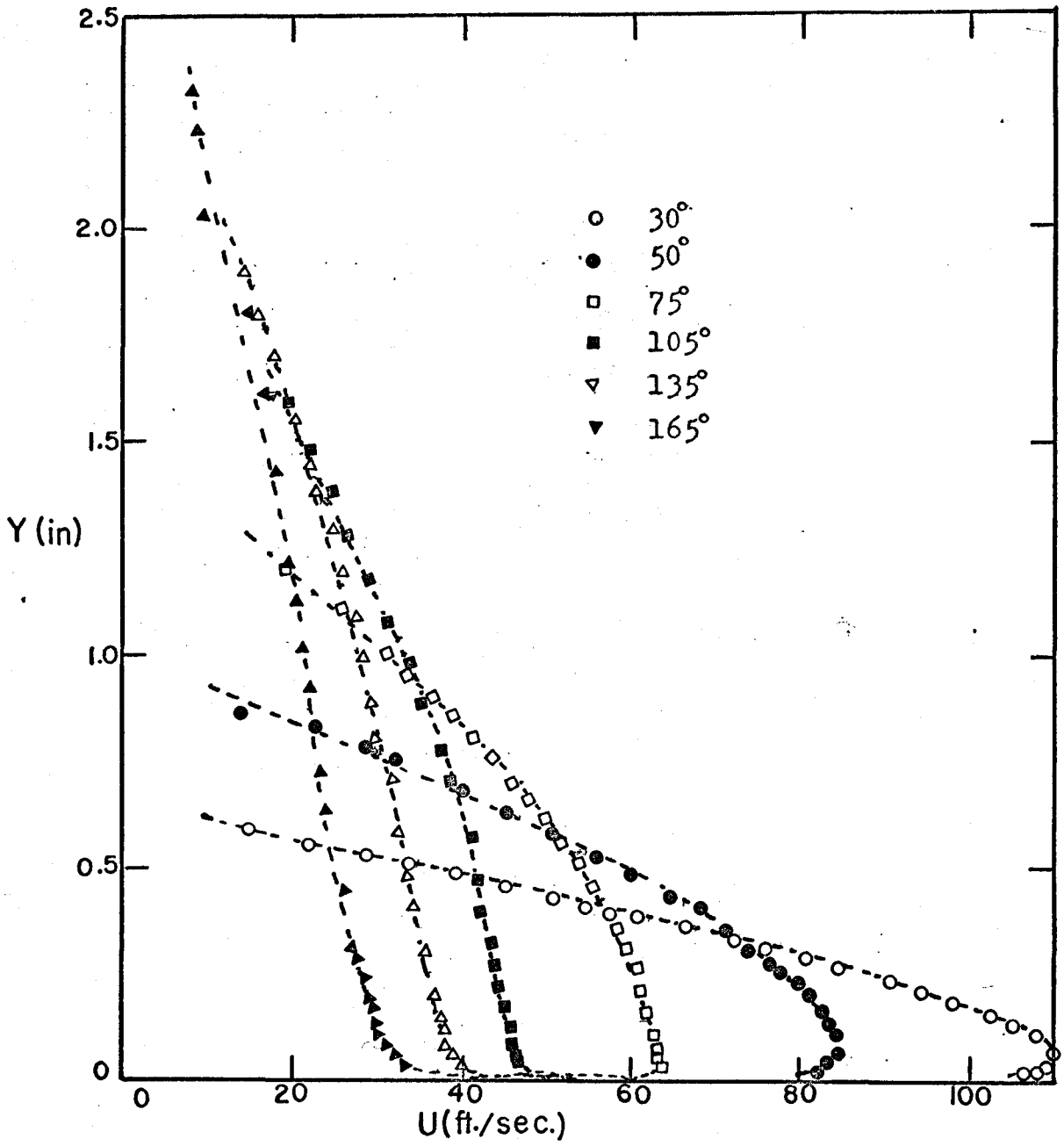

Fig. 5.8 DIMENSIONAL VELOCITY PROFILES (N = 1000)

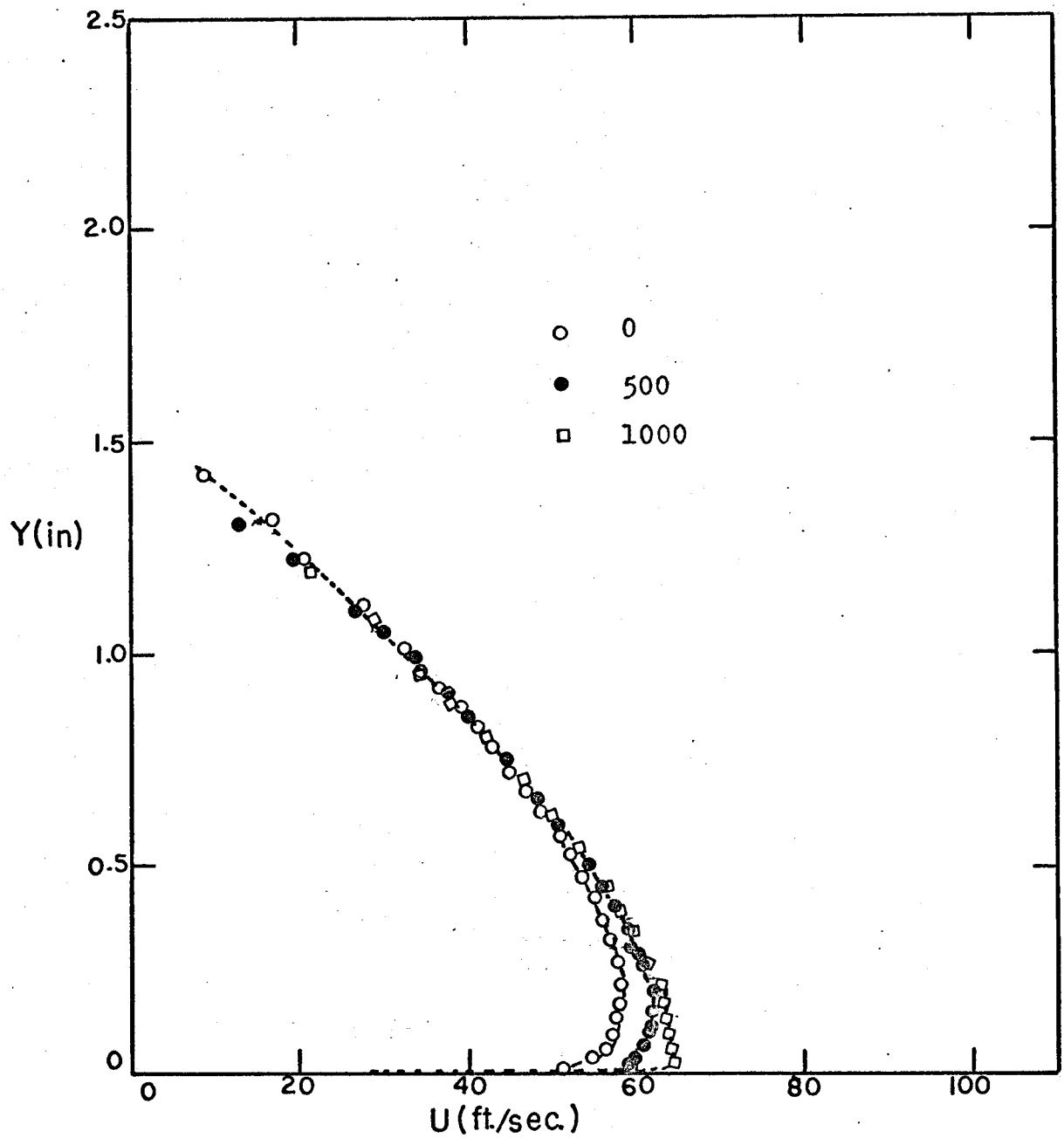

Fig. 5.9 EFFECT OF ROTATION ON DIMENSIONAL VELOCITY PROFILE

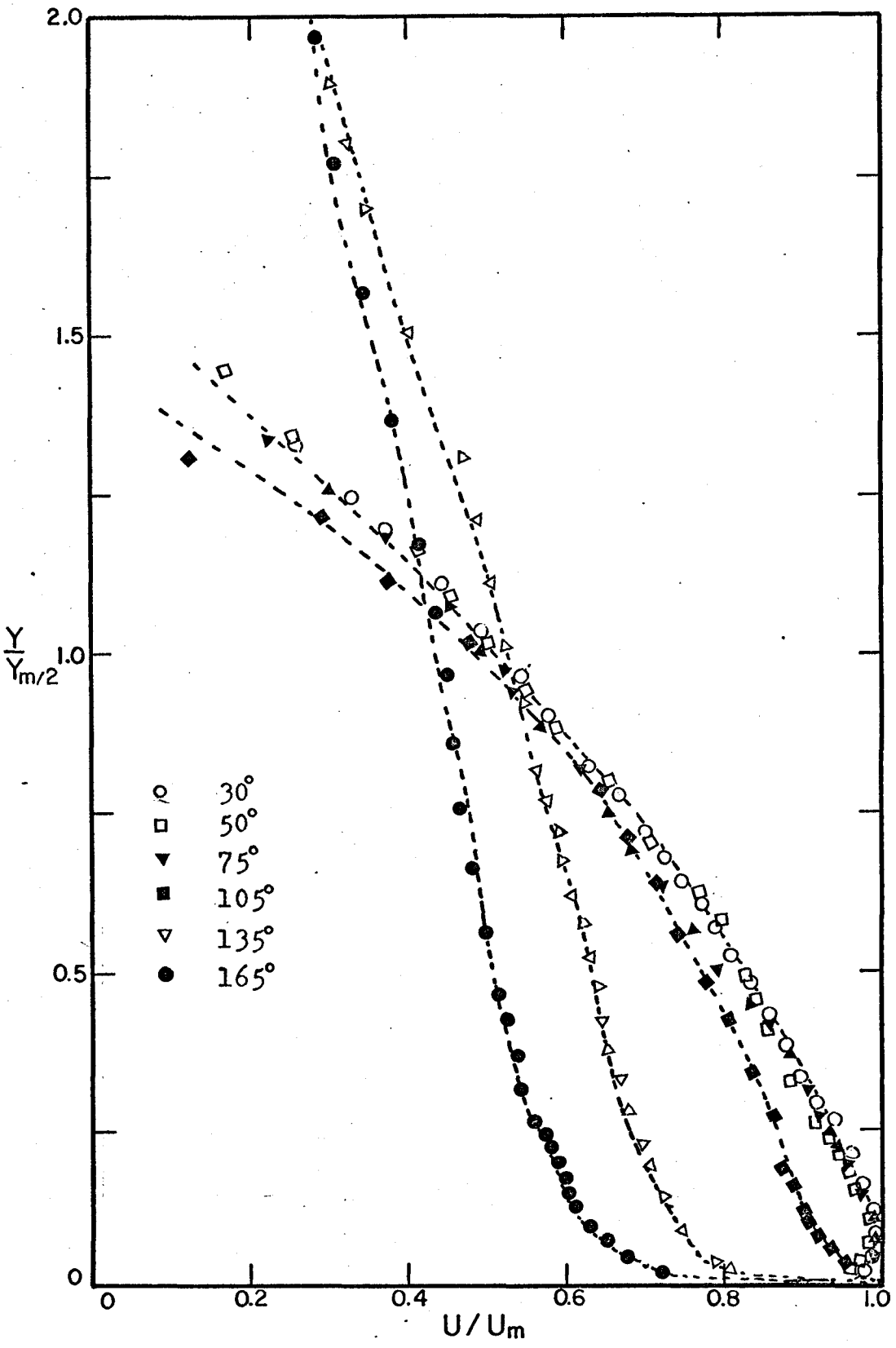

Fig. 5.10 NON-DIMENSIONAL VELOCITY PROFILES (N = 800)

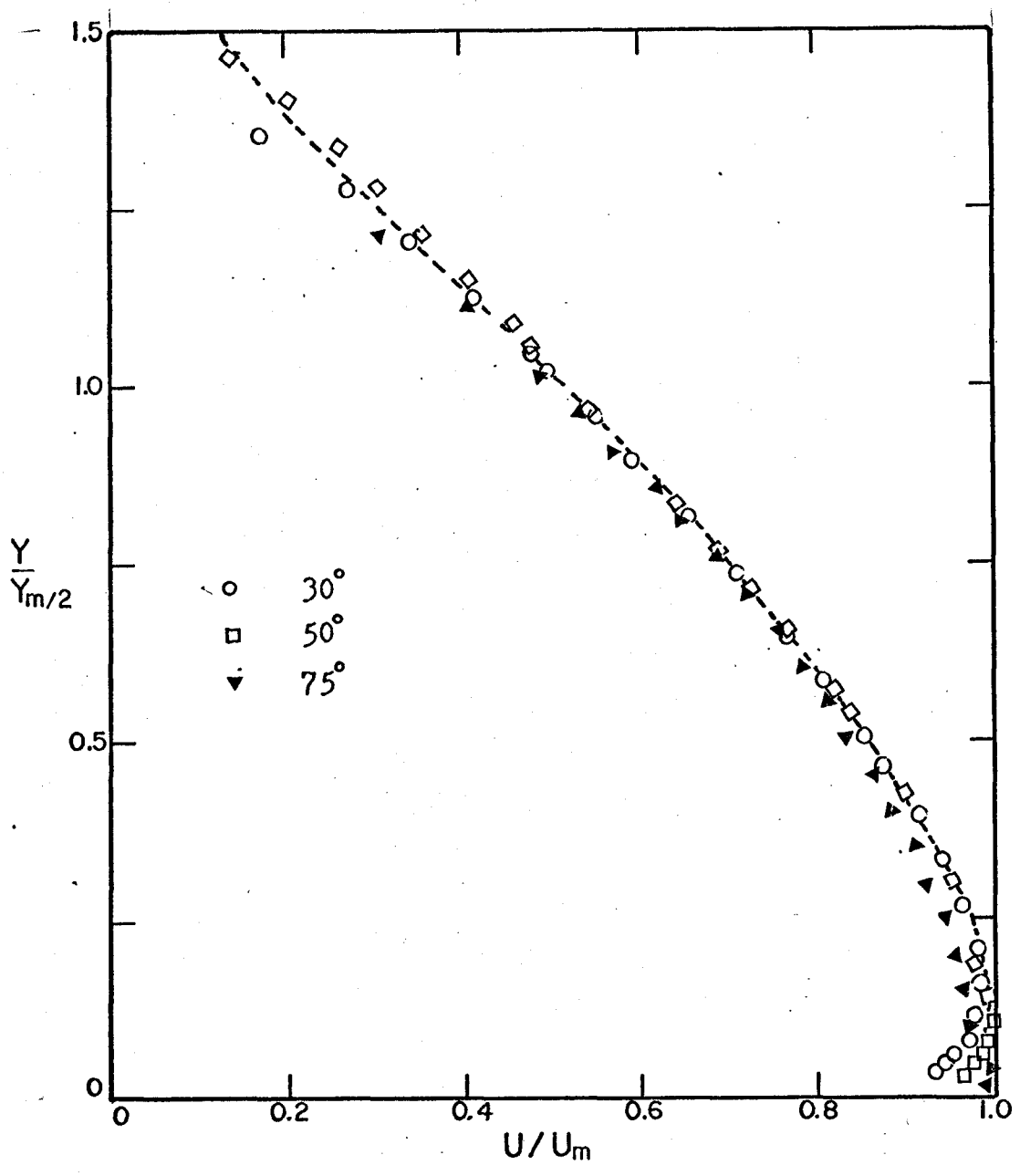

Fig. 5.11 NON-DIMENSIONAL VELOCITY PROFILES (N - 1000)

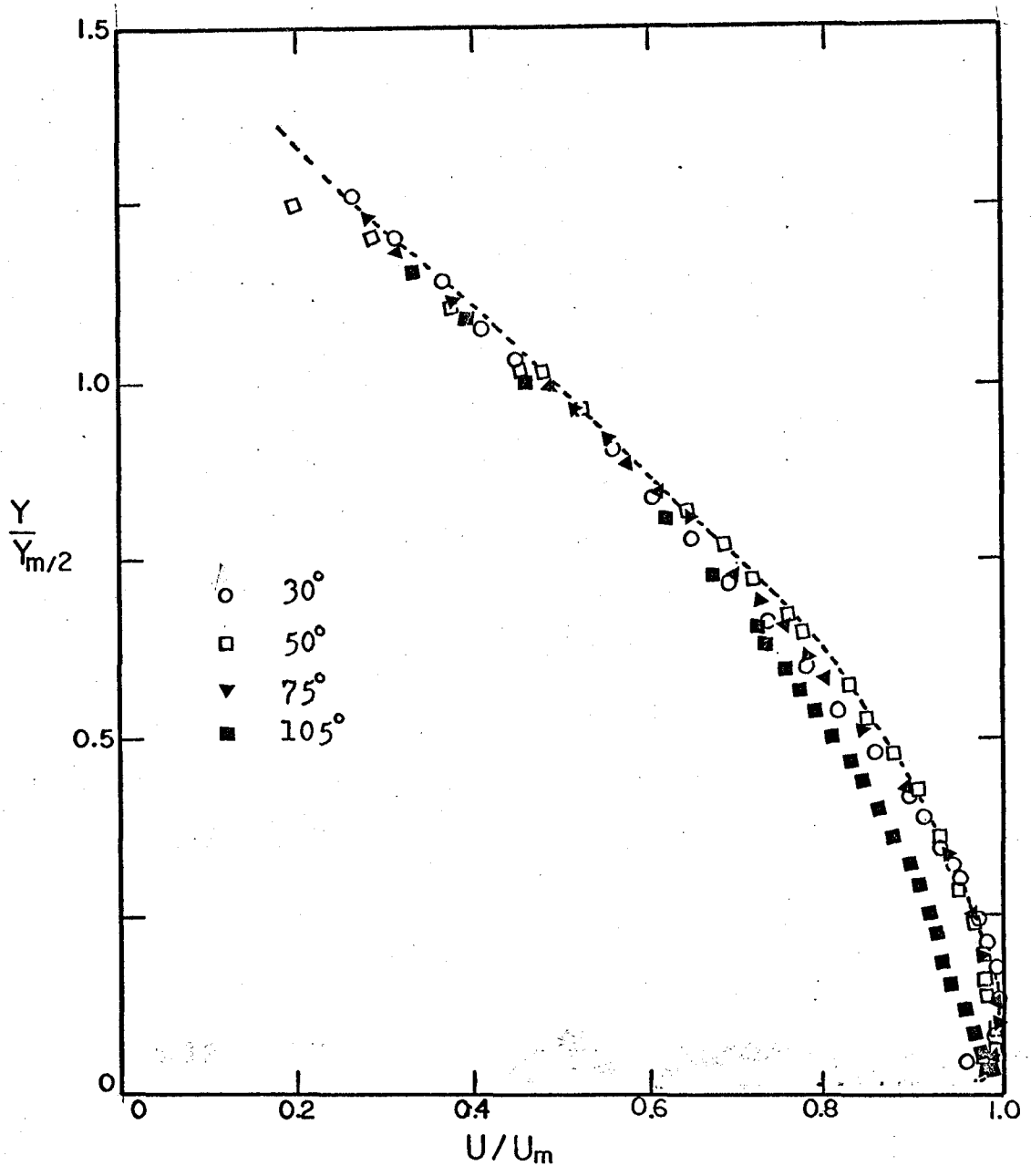

Fig. 5.12 NON - DIMENSIONAL VELOCITY PROFILES (N = 700)

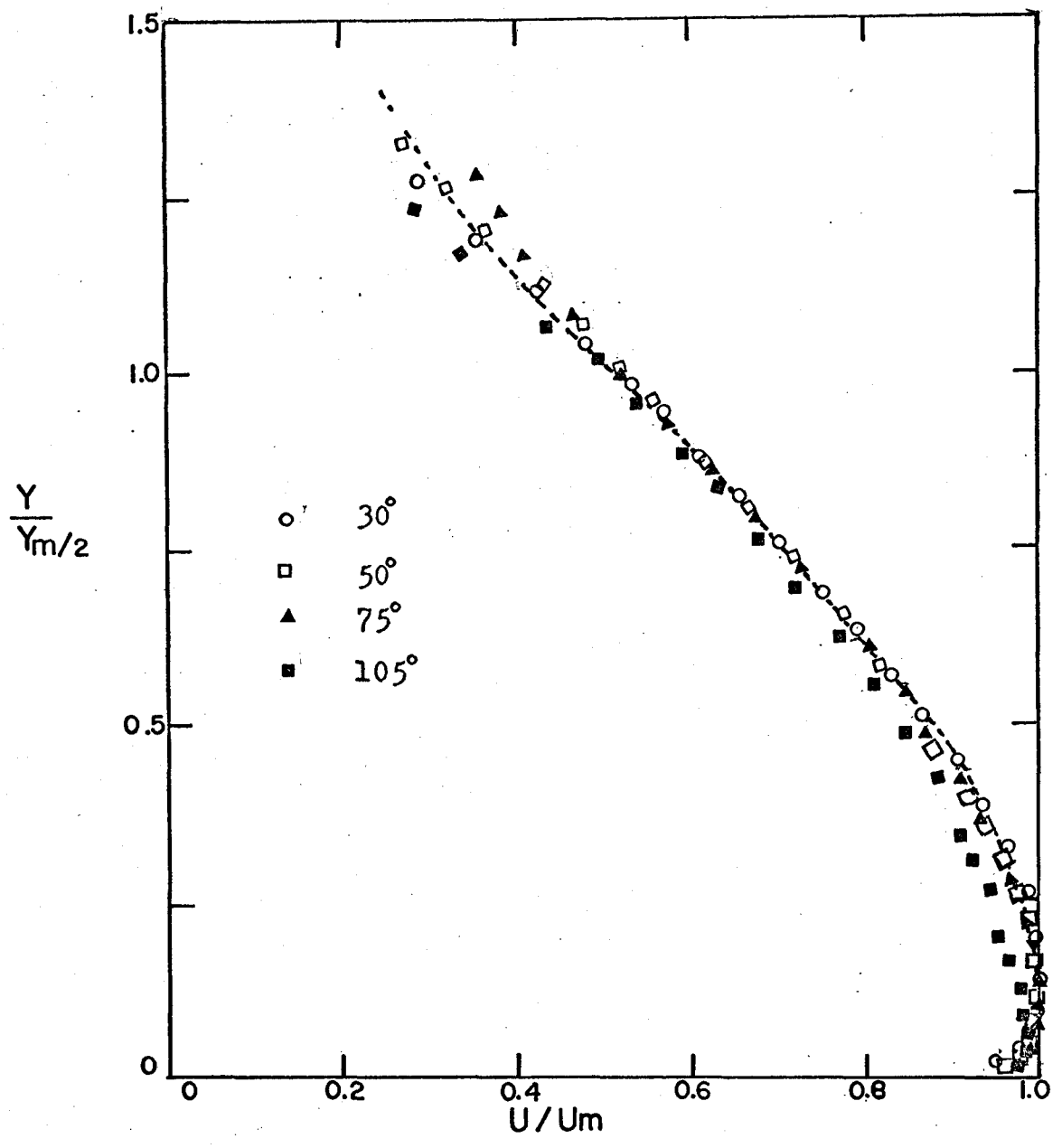

Fig. 5.13 NON-DIMENSIONAL VELOCITY PROFILES (N = 500)

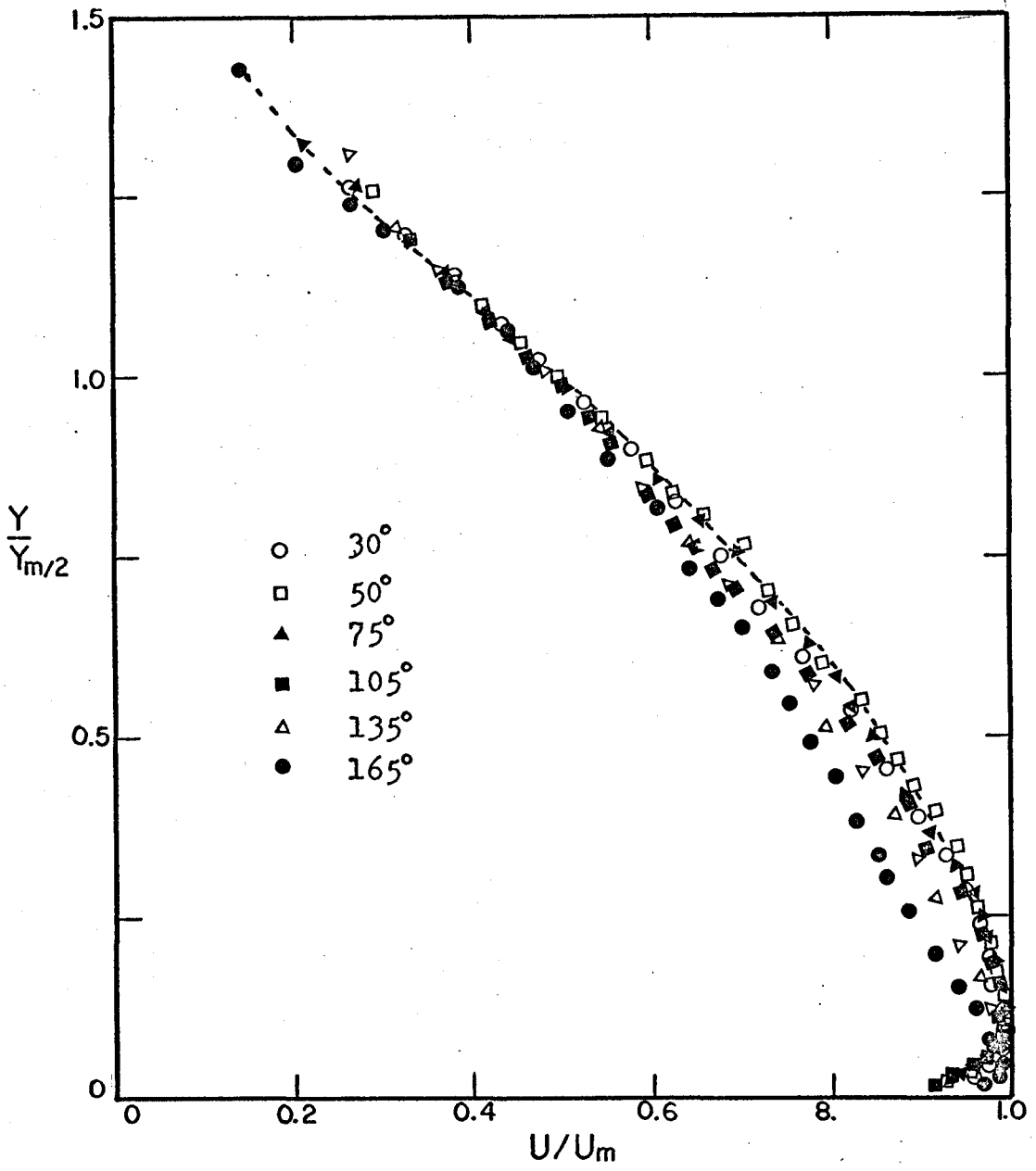

Fig. 5.14 NON-DIMENSIONAL VELOCITY PROFILES (N = 350)

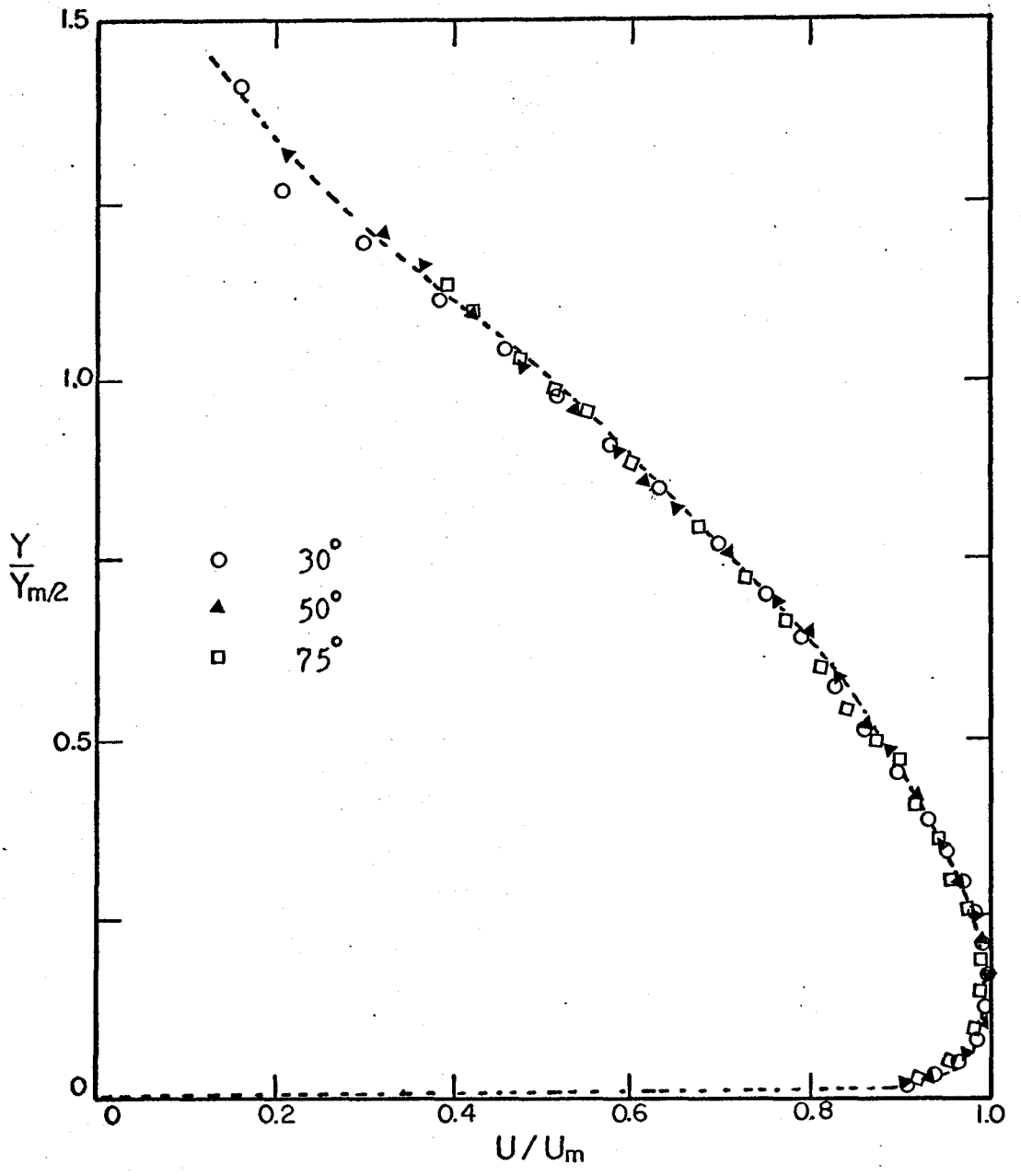

Fig. 5.15 NON-DIMENSIONAL VELOCITY PROFILES (N = 0)

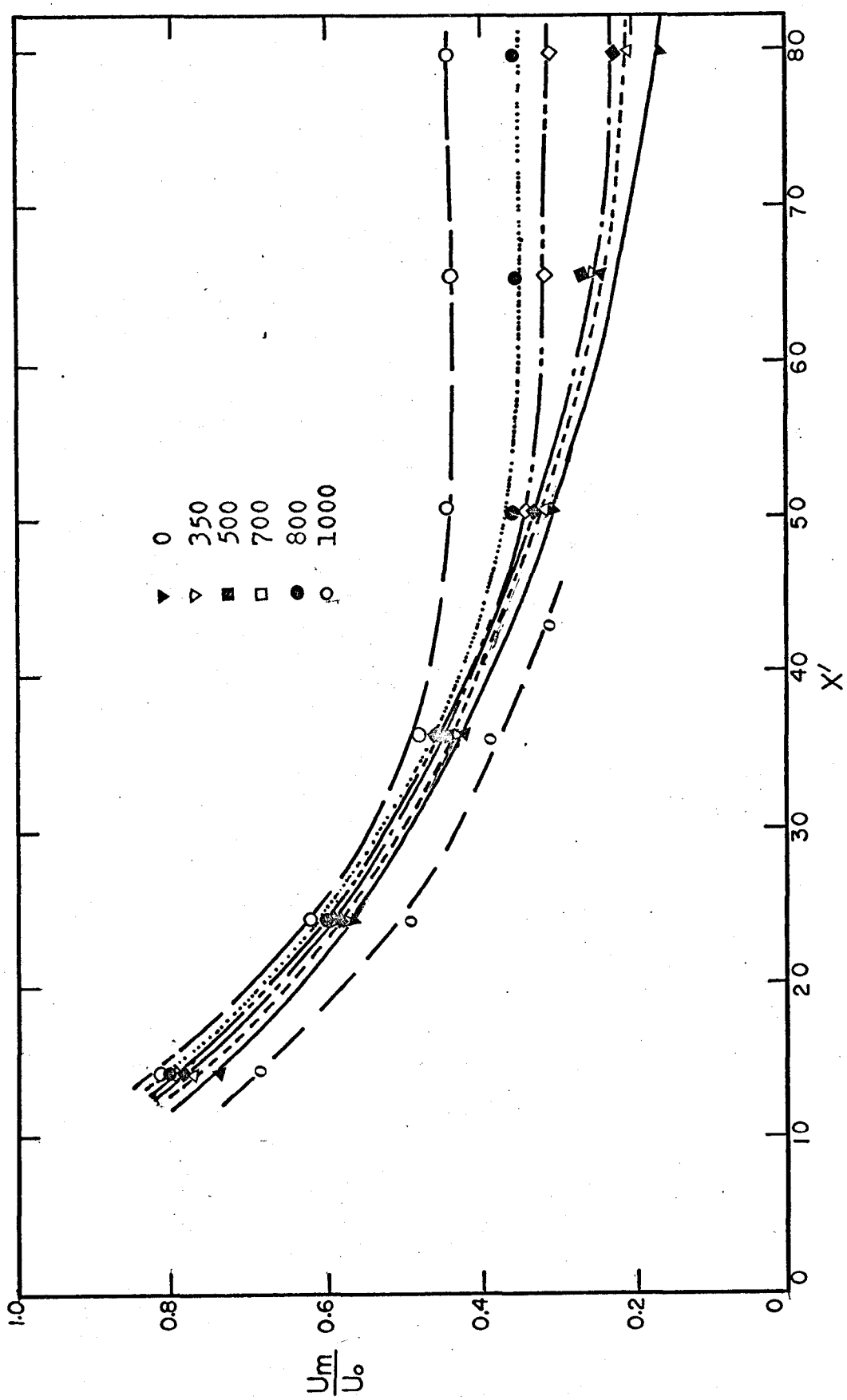

Fig. 5.16 MAXIMUM VELOCITY DECAY

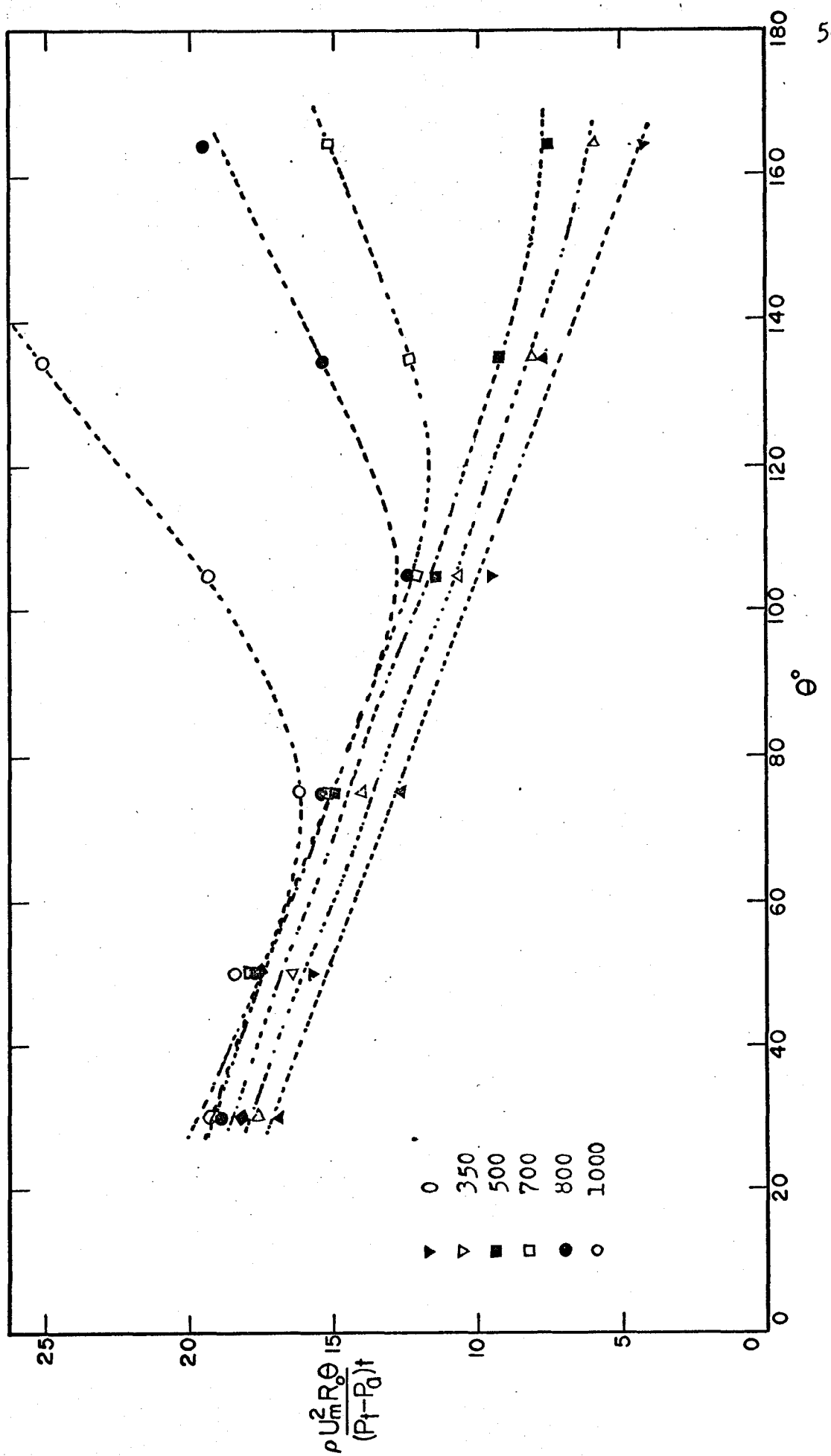

Fig. 5.17 PLOT OF MAXIMUM VELOCITY COEFFICIENTS VS. θ

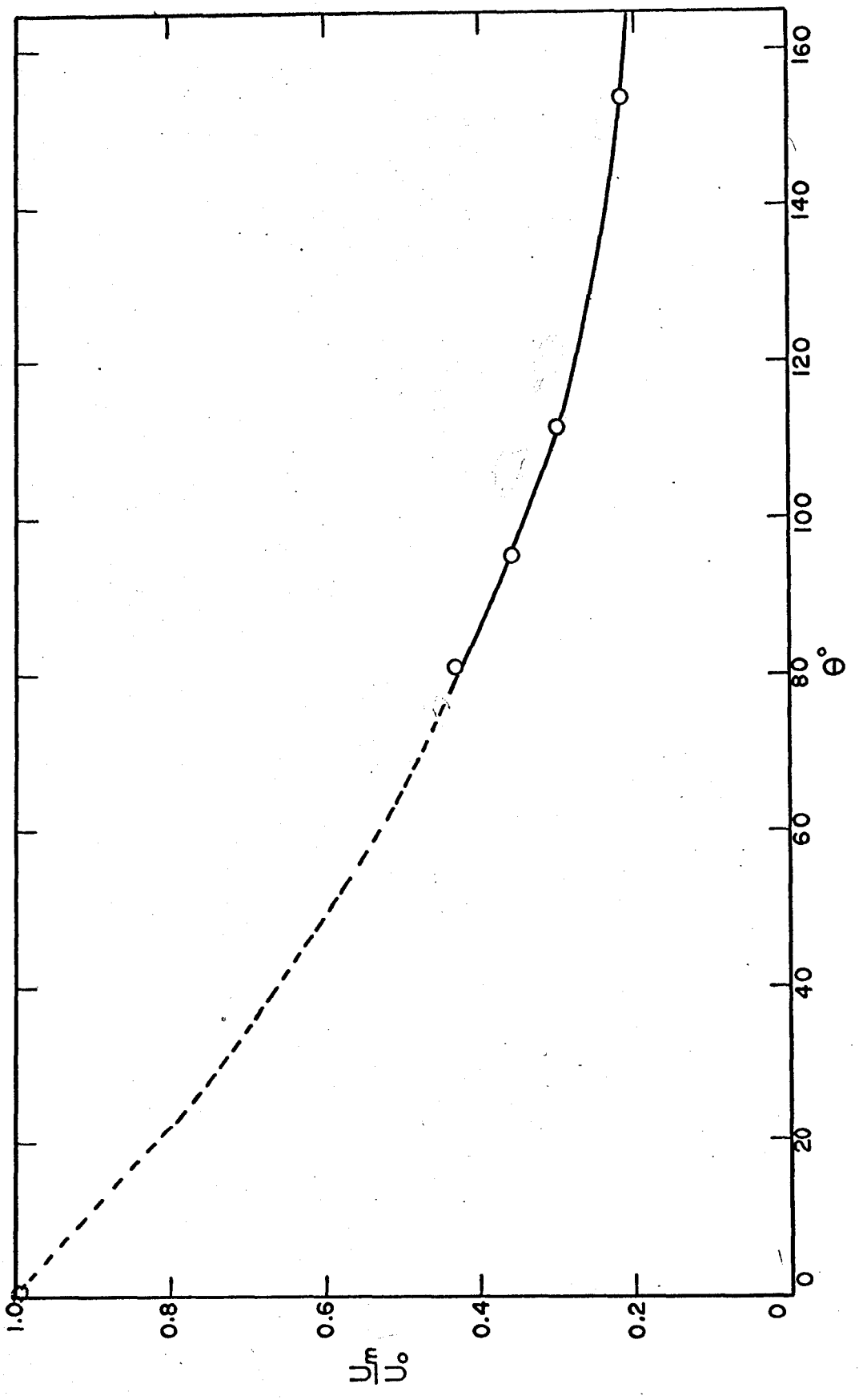

Fig. 5.18 EFFECT OF ROTATION ON THE UPPER LIMIT OF REGION II

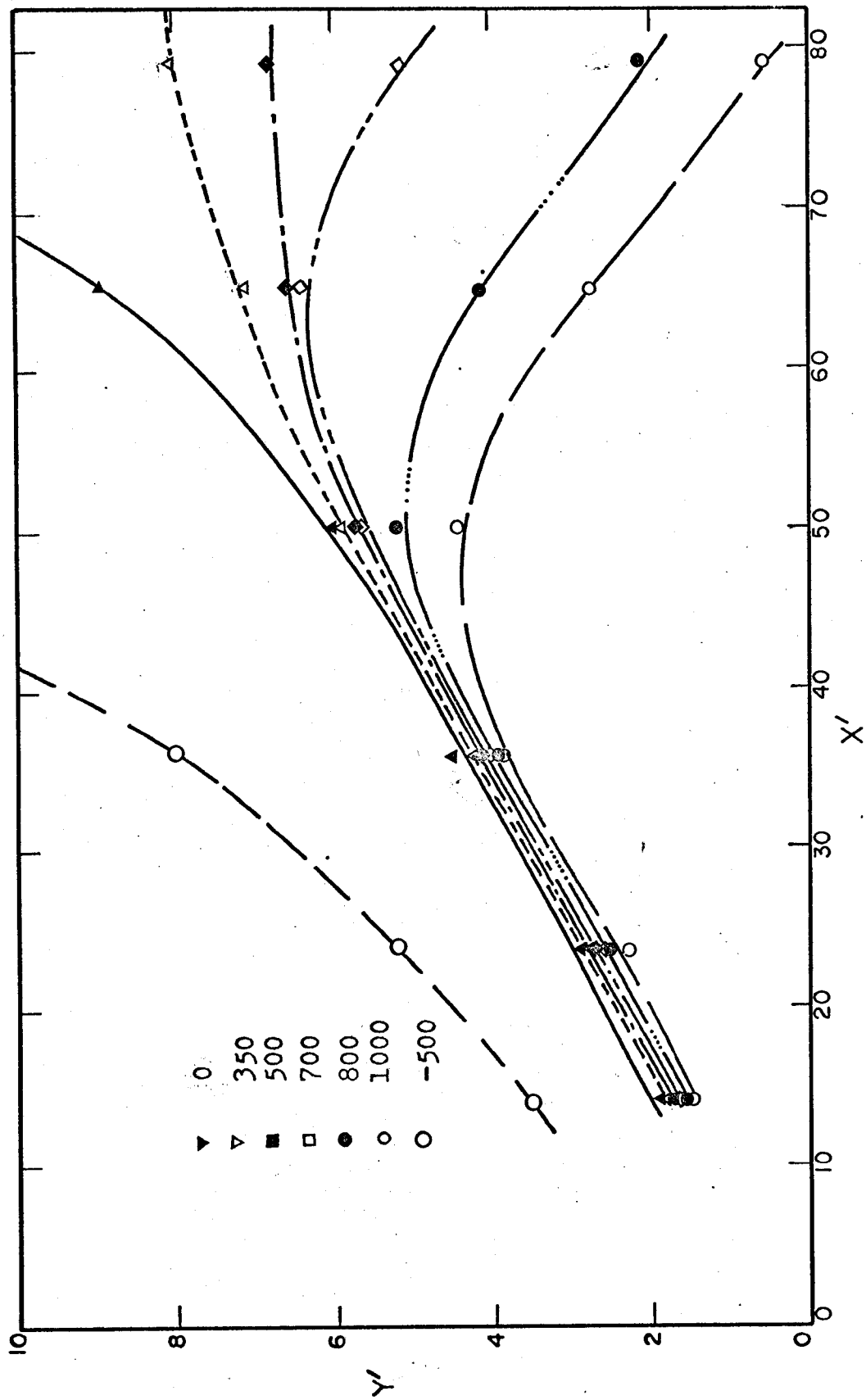

Fig. 5.19 JET GROWTH

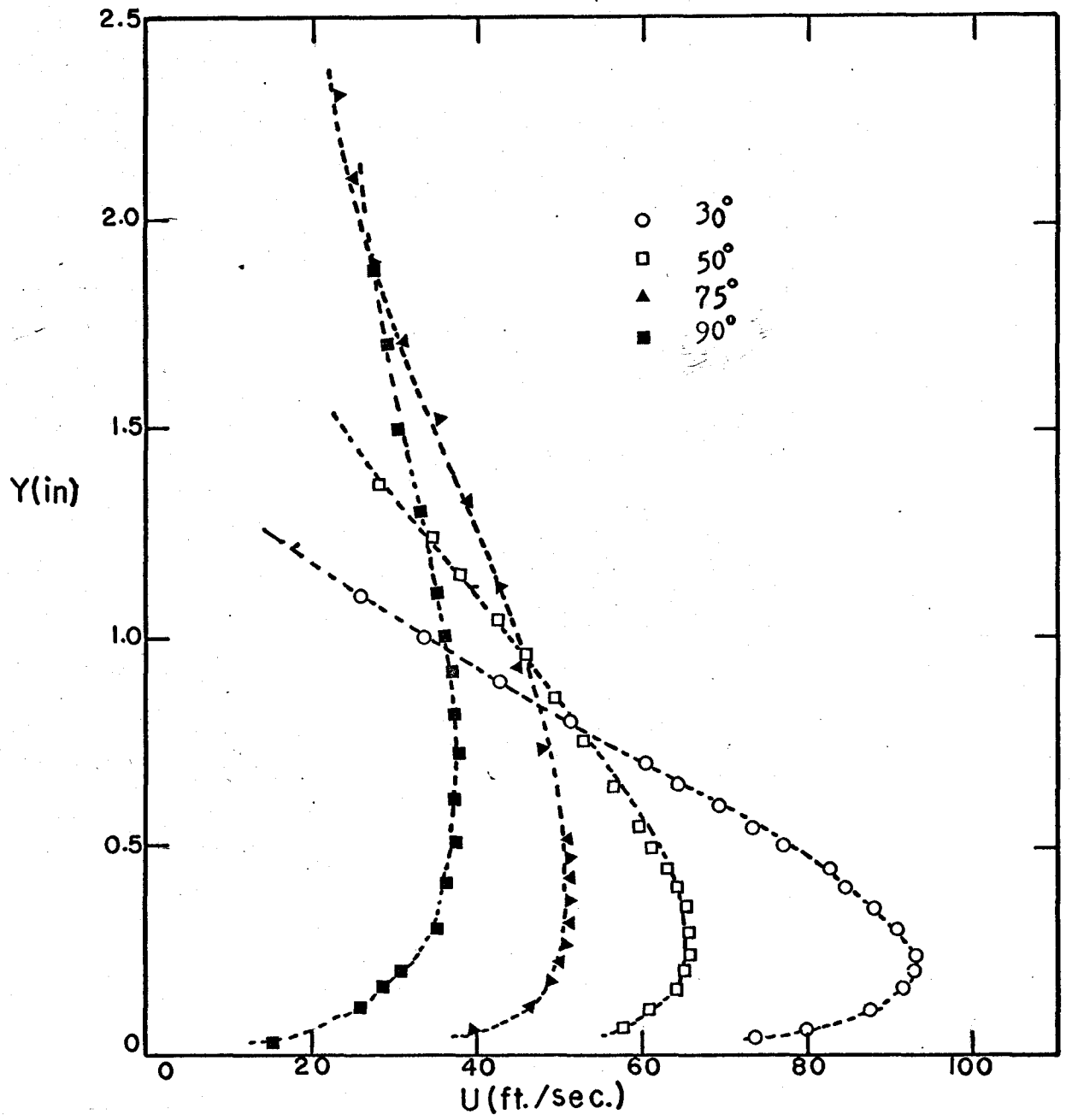

Fig. 5.20 DIMENSIONAL VELOCITY PROFILES
(OPPOSITE ROTATION N = 500)

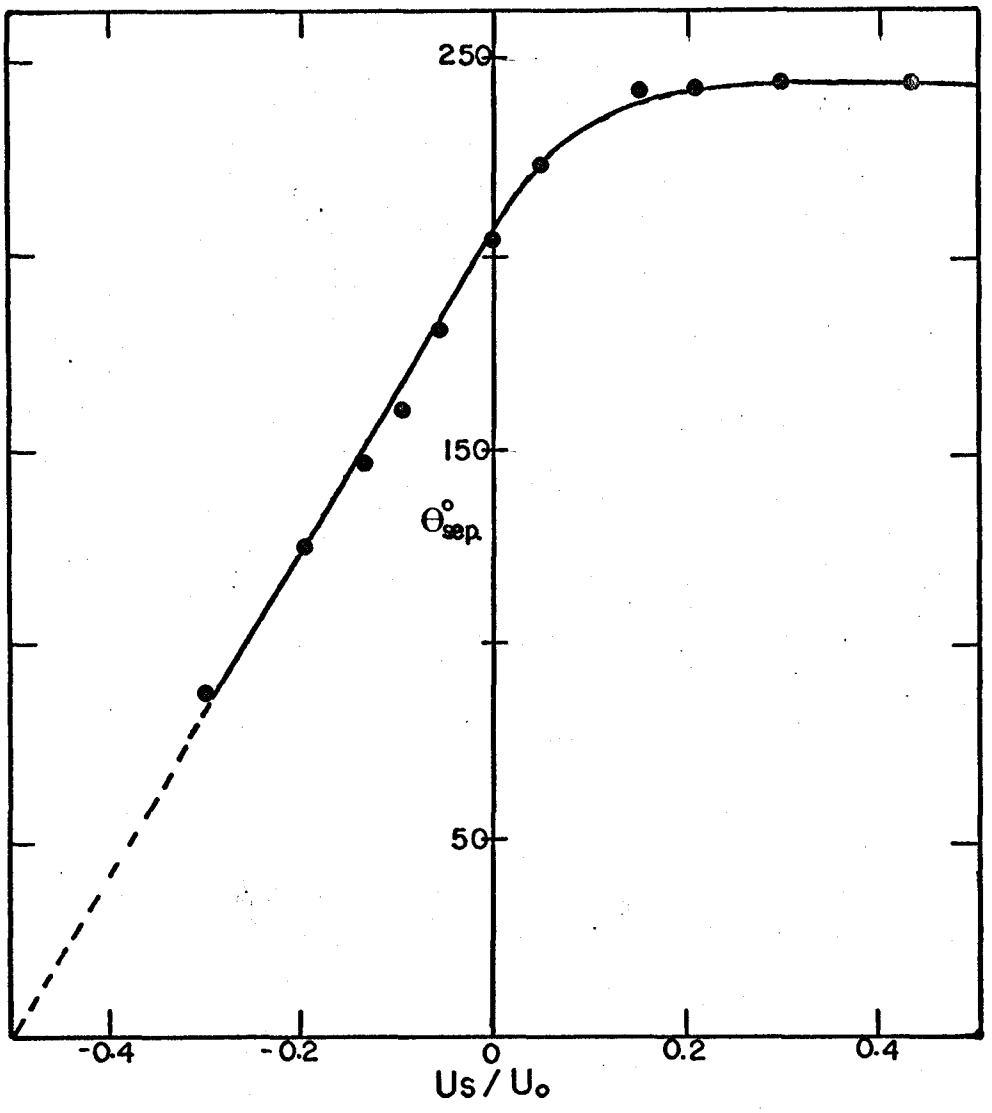

Fig. 5.21 EFFECT OF ROTATION ON $\theta_{sep.}$

APPENDIX

For the present investigation, it is assumed that the following relation is true:

$$\theta_{sep} = f\,[(Pt - Pa), \varrho, \nu, t, Ro, w]$$

In the M. L. T. system of units, the dimensional matrix for the parameters is:

	1	2	3	4	5	6	7
	θ_{sep}	ν	Ro	t	(Pt-Pa)	ϱ	w
M	0	0	0	0	1	1	0
L	0	2	1	1	-1	-3	0
T	0	-1	0	0	-2	0	-1

The rank (r) of the matrix is three (3) and since there are seven (7) variables, the number of dimensionless groups is $7 - 3 = 4$.

Treating the present problem as jet controlled flow, the repeating variables selected are (Pt - Pa), ϱ, Ro. The dimensionless groups can be expressed as:

$$II_1 = \theta_{sep}$$

$$II_2 = (Pt - Pa)^{x_2}\ \varrho^{y_2}\ Ro^{z_2}\ \nu$$

$$II_3 = (Pt - Pa)^{x_3}\ \varrho^{y_3}\ Ro^{z_3}\ t$$

$$II_4 = (Pt - Pa)^{x_4} \rho^{y_4} Ro^{z_4} w$$

Further, the dimensionless group are:

$$II_1 = \theta_{sep}$$

$$II_2 = \left[\frac{(Pt - Pa)Ro^2}{\rho \nu^2}\right]^{\frac{1}{2}}$$

$$II_3 = \frac{t}{Ro}$$

$$II_4 = \frac{\rho^{\frac{1}{2}} Ro\, w}{(Pt - Pa)} = \frac{Us}{Uo}$$

Hence the relationship can be written as

$$\theta_{sep} = f\left\{\left[\frac{(Pt - Pa)Ro^2}{\rho \nu^2}\right]^{-\frac{1}{2}}, \frac{t}{Ro}, \frac{Us}{Uo}\right\}$$

Dividing II_2 by II_3, we get the dimensionless group as:

$$II_6 = \frac{II_2}{II_3} = \left[\frac{(Pt - Pa)tRo}{\rho \nu^2}\right]^{-\frac{1}{2}}$$

If the position of separation is sufficiently far from the slot

$$\theta_{sep} = f\left\{\left[\frac{(Pt - Pa)tRo}{\rho \nu^2}\right]^{\frac{1}{2}}, \frac{Us}{Uo}\right\}$$

VITA AUCTORIS

1943 Born in Yugoslavia on August 18.

1963 Completed high school at Essex District High School, Essex, Ontario in June.

1967 Received the degree of Bachelor of Applied Science in Mechanical Engineering from the University of Windsor, Windsor, Ontario.

1968 Currently a candidate for the Degree of Master of Applied Science in Mechanical Engineering at the University of Windsor.